

1 **A NOVEL MECHANISM FOR NF- κ B-ACTIVATION VIA I κ B-AGGREGATION: IMPLICATIONS**
2 **FOR HEPATIC MALLORY-DENK-BODY INDUCED INFLAMMATION**

3
4 **Yi Liu¹, Michael J. Trnka², Shenheng Guan², Doyoung Kwon¹, Do-Hyung Kim³, J-J. Chen⁴,**
5 **Peter A. Greer⁵, A. L. Burlingame², and Maria Almira Correia^{1,2,6,7}**

6
7 Departments of Cellular & Molecular Pharmacology¹, Pharmaceutical Chemistry², and
8 Bioengineering and Therapeutic Sciences⁶, and The Liver Center⁷,
9 University of California San Francisco, San Francisco CA 94158-2517,

10 Departments of Biochemistry, Molecular Biology, and Biophysics³, University of Minnesota,
11 Minneapolis, MN55455,

12 Institute for Medical Engineering and Science ⁴, MIT, Cambridge, MA, 02139

13 Department of Pathology and Molecular Medicine⁵, *Queen's* University; Kingston, ON; K7L 3N6

14
15 **Running title: *NF- κ B-activation upon PPIX-elicited I κ B-sequestration***

16
17 Address correspondence to: M. A. Correia, Mission Bay Campus, Genentech Hall, 600 16th
18 Street, Box 2280, University of California San Francisco, San Francisco, CA 94158-2517.
19 FAX: 415-476-5292. E-mail: almira.correia@ucsf.edu

20
21 **Keywords:** Mallory-Denk-bodies, I κ B α , I κ B β , NF- κ B, p62, erythropoietic protoporphyria, X-
22 linked protoporphyria, liver inflammation, NMPP, PPIX, ZnPPIX, proteomics.

23
24 **Conflict of interest:** The authors have no conflict of interest to declare.

25
26 **Financial Support:** These studies were supported by NIH Grants DK26506 (MAC), GM44037
27 (MAC), GM25515 (POM), GM097057 (DHK), DK087984 (JJC), and CIHR grant #81189 (PAG).
28 We also acknowledge the UCSF Bio-Organic Biomedical Mass Spectrometry Resource (Prof. A.
29 L. Burlingame, Director) supported by the Adelson Medical Research Foundation.

30

31 **Author Contributions:**

32 Y.L and M.A.C designed the studies and wrote the manuscript. M.A.C supervised the project.

33 Y.L conducted most of the experiments with MS support and interpretation from M.T. and S.G.

34 D.K. carried out the ZnPP *in vivo* mouse experiments. D.Y.K, J.J.C, and P.A.G provided critical,

35 *sine qua non* research materials. All authors critically reviewed the manuscript.

36

37

38

39

40

41

42

43

44

45

46

47 **ABSTRACT**

48

49 **Background & Aims:**

50 Mallory-Denk-bodies (MDBs) are hepatic protein aggregates associated with inflammation both
51 clinically and in MDB-inducing models. Similar protein aggregation in neurodegenerative
52 diseases also triggers inflammation and NF- κ B activation. However, the precise mechanism that
53 links protein aggregation to NF κ B-activation and inflammatory response remains unclear.

54

55 **Methods:**

56 Herein, we find that treating primary hepatocytes with MDB-inducing agents (N-
57 methylprotoporphyrin, protoporphyrin IX (PPIX), or ZnPPIX) elicited an I κ B α -loss with
58 consequent NF- κ B activation. We characterized the underlying mechanism in detail using
59 hepatocytes from various knockout mice and MEF cell lines and multiple approaches including
60 immunoblotting, EMSA, RT-PCR, confocal immunofluorescence microscopy, affinity
61 immunoprecipitation, and protein solubility assays. Additionally, we performed rigorous
62 proteomic analyses to identify the proteins aggregating upon PPIX treatment and/or co-
63 aggregating with I κ B α .

64

65 **Results:**

66 Four known mechanisms of I κ B α -loss were probed and excluded. Immunofluorescence
67 analyses of ZnPPIX-treated cells coupled with 8 M urea/CHAPS-extraction revealed that this
68 I κ B α -loss was due to its sequestration along with I κ B β into insoluble aggregates. Through
69 proteomic analyses we identified 47 aggregation-prone proteins that co-aggregate with
70 I κ B α through direct interaction or proximity. Of these ZnPPIX-aggregation targets, the

71 nucleoporins Nup153 and Nup358/RanBP2 were identified through RNA-interference, as likely
72 mediators of I κ B α -nuclear import.

73

74 **Conclusion:**

75 We discovered a novel mechanism of inflammatory NF- κ B activation through I κ B-sequestration
76 into insoluble aggregates along with interacting aggregation-prone proteins. This mechanism
77 may account for the protein aggregate-induced inflammation observed in MDB-associated liver
78 diseases, thereby identifying novel targets for therapeutic intervention. Because of inherent
79 commonalities this MDB cell model is a *bona fide* protoporphyric model, making these findings
80 equally relevant to the liver inflammation associated with clinical protoporphyria.

81

82 **Lay Summary:**

83 Mallory-Denk-bodies (MDBs) are hepatic protein aggregates commonly featured in many liver
84 diseases. MDB-presence is associated with the induction of inflammatory responses both
85 clinically and in all MDB-inducing models. Similar protein aggregation in neurodegenerative
86 diseases is also known to trigger inflammation and NF κ B pathway activation via an as yet to be
87 characterized non-canonical mechanism. Herein using a MDB-inducing cell model, we
88 uncovered a novel mechanism for NF κ B activation via cytosolic I κ B-sequestration into insoluble
89 aggregates. Furthermore, using a proteomic approach, we identified 47 aggregation-prone
90 proteins that interact and co-aggregate with I κ B α . This novel mechanism may account for the
91 protein aggregate-induced inflammation observed in liver diseases, thereby identifying novel
92 targets for therapeutic intervention.

93

94 INTRODUCTION

95 Protein aggregates and inclusion bodies are linked to various neurodegenerative,
96 muscular and hepatic diseases [Alzheimer's, Parkinson's, Desmin-related myopathies, and
97 Mallory-Denk-bodies (MDBs) [1]]. Although different aggregates vary with each tissue source
98 and in predominant protein composition, they contain common components such as
99 p62/Sequestosome-1, ubiquitin, chaperones and proteasome constituents, which are often
100 misfolded, highly insoluble, and cross-linked [1, 2].

101 Hepatic MDBs consisting largely of phosphorylated cytokeratins and p62 are commonly
102 found in patients with alcoholic steatohepatitis (ASH) and non-alcoholic steatohepatitis (NASH),
103 primary biliary cirrhosis, non-alcoholic cirrhosis, hepatocellular carcinoma, morbid obesity, and
104 copper-related disorders [3]. MDBs can be reproduced in mice by long term feeding of
105 griseofulvin (GF) or 3,5-dicarbethoxy-1,4-dihydrocollidine (DDC) [4, 5]. Both compounds
106 inactivate certain hepatic cytochromes P450, converting their prosthetic heme into N-
107 methylprotoporphyrin(s) (NMPP) that inhibit hepatic ferrochelatase (Fech) resulting in hepatic
108 heme depletion and protoporphyrin IX (PPIX) accumulation [6, 7] (Fig. 1A). $Fech^{m1Pas}$ mutant
109 (*fech/fech*) mice with <5% of normal enzyme activity also develop spontaneous MDBs at 20-
110 weeks of age, validating their use as an experimental model for MDB induction [8].

111 ASH and NASH patient liver histology reveals that MDBs are associated with
112 inflammatory responses, with MDB-containing hepatocytes often surrounded by neutrophils [1,
113 9]. All MDB-inducing mouse models also accumulate hepatic PPIX and exhibit liver inflammation
114 and injury at an early stage when MDBs are not yet visible [10, 11]. Cumulative biochemical
115 evidence indicates that in these mouse models as well as in DDC-, NMPP- or PPIX-treated cell
116 models, certain proteins such as p62, cytokeratins CK8/18 and lamin begin to aggregate at a
117 much earlier stage before MDBs are detected [12, 13]. Similarly, many neurodegenerative
118 diseases are also associated with inflammation at an early stage, and amyloid protein

119 aggregation has been shown to initiate an inflammatory response [14]. Moreover, induction of
120 various protein aggregates, as in myofibrillar myopathy and Amyotrophic Lateral Sclerosis (ALS),
121 triggers the activation of NF- κ B (nuclear factor kappa-light-chain-enhancer of activated B cells)
122 via a noncanonical pathway independent of I κ B α -phosphorylation/degradation [15]. However,
123 the precise molecular link between protein aggregation and NF- κ B-activation and inflammatory
124 response remains unclear.

125 Of the existing NF- κ B/Rel transcription factors [16], p65/p50 is not only the most
126 ubiquitous and biologically active NF- κ B-heterodimer, but also the major hepatic species [17].
127 p65/p50 is normally sequestered in the cytoplasm by NF-kappa-B inhibitors (I κ B). Of these, in
128 human hepatocytes, HepG2 cells and cultured mouse hepatocytes, I κ B α and I κ B β are the major
129 forms, each regulated by different signals [18-21]. I κ B-binding masks NF- κ B nuclear localization
130 signal (NLS) and DNA-binding domain [16]. Signal-induced I κ B-unleashing of cytoplasmic NF-
131 κ B most commonly via phosphorylation and subsequent ubiquitin-dependent degradation (UPD)
132 of both I κ B α and I κ B β [22-24], results in the nuclear translocation of DNA-binding competent
133 NF- κ B, with consequent transcriptional activation of its target genes including that of I κ B α [25],
134 but not of I κ B β [26]. I κ B α is then rapidly *de novo* oversynthesized (overshoot), and following
135 nuclear import, binds and displaces the DNA-bound NF- κ B, masking its NLS and accelerating
136 its nuclear export, required for down regulation and eventual termination of NF- κ B-mediated
137 transcriptional activation [27]. Thus, while both hepatic I κ Bs are largely involved in NF- κ B-
138 cytoplasmic retention, only I κ B α is involved in nuclear NF- κ B-transcriptional suppression [19]

139 Our findings herein reveal a loss of I κ B α and I κ B β with subsequent NF- κ B activation
140 upon treatment of primary hepatocytes with NMPP (an established MDB inducer), or ZnPPIX
141 (ZnPP). We probed the role of four plausible mechanisms for NF- κ B-activation via reduction of
142 intracellular I κ B α -levels in this NMPP-elicited I κ B α -loss and excluded them all (Supplementary

143 Results). Instead, we found that this apparent I κ B α -loss upon NMPP- or ZnPP-treatment is
144 actually due to its phase sequestration into insoluble cellular aggregates along with I κ B β , as well
145 as the nucleoporins Nup153 and Nup358 that are involved in I κ B α nuclear import and
146 subsequent termination of NF- κ B activation.

147 To our knowledge, this is the first evidence that NF- κ B is also activated through I κ B-
148 sequestration into insoluble aggregates. We believe such a novel mechanism accounts for the
149 persistent hepatic NF- κ B activation that may directly contribute to the severe inflammatory
150 responses and liver injury observed not only in various MDB-featuring liver diseases and
151 experimental MDB-models but also in acute erythropoietic protoporphyria (EPP) and X-linked
152 protoporphyria (XLPP) [28-30].

153

154 RESULTS

155 ***NMPP-elicited PPIX accumulation with concurrent I κ B α -loss and NF- κ B activation in***
156 ***cultured mouse hepatocytes:*** NMPP-treatment of cultured mouse hepatocytes as expected
157 from its ferrochelatase inhibition, resulted in cellular PPIX accumulation (Fig. 1A). In parallel, a
158 gradual I κ B α loss was also observed in hepatic lysates upon NMPP-treatment (Fig. 1B). This
159 I κ B α -loss was reversed upon inclusion of hemin, but not that of the proteasomal inhibitor MG-
160 132, or the dual autophagic-lysosomal degradation (ALD) inhibitors 3-methyladenine (3MA) +
161 NH₄Cl. These findings thus excluded both UPD and ALD involvement in this I κ B α -loss. Further
162 supportive evidence was provided by studies in HepG2 cells transfected with a S₃₂A/S₃₆A-I κ B α
163 mutant that is resistant to phosphorylation and UPD (Fig. S1A) as NMPP caused a similar time-
164 dependent loss of both WT I κ B α and its mutant. Parallel EMSA of nuclear extracts from these
165 NMPP-treated hepatocytes revealed a time-dependent hepatic NF- κ B activation, indicating that
166 this hepatic I κ B α loss was indeed physiologically relevant (Figs. 1C & S1B). This NF- κ B

167 activation was also attenuated by hemin (Fig. 1C), consistent with the hemin-mediated inhibition
168 of I κ B α loss (Fig. 1B). These findings suggested that this culture model was a valid model to
169 interrogate the association of PPIX accumulation with NF- κ B-activation and inflammation.

170

171 Four additional mechanisms -- two established and two plausible -- for NF- κ B-activation via
172 reduction of intracellular I κ B α -levels [i.e. (i) translational suppression by heme-deficiency-
173 triggered heme-regulated inhibitor (HRI) eIF2 α kinase-activation ([31]; Figs. 1D & S2A); (ii)
174 enhanced autophagy ([32]; Fig. S2B); (iii) enhanced calpain-mediated proteolysis ([33];
175 Fig.S2C); and (iv) PPIX-photoactivation and consequent ROS-mediated oxidative stress [28] in
176 NMPP-elicited I κ B α -loss (Supplementary Results; Fig. S3), were all probed and excluded.

177

178 ***PPIX and ZnPP are even more potent inducers of I κ B α -loss, NF- κ B-activation and p62***
179 ***oligomerization/aggregation than NMPP:*** Because NMPP-elicited ferrochelatase inhibition
180 results in PPIX-accumulation, we examined whether this accumulation (and not heme
181 deficiency) was mainly responsible for the observed I κ B α loss and NF- κ B activation. We
182 observed a greater I κ B α loss after either PPIX or ZnPP relative to that seen with NMPP alone
183 (Fig. 1E). While the NMPP-elicited I κ B α loss was to a great extent prevented by hemin
184 inclusion, the I κ B α loss after PPIX or ZnPP was not (Fig. 1E; see Supplementary Discussion).
185 EMSA analyses revealed a NF- κ B activation that was proportional to the observed I κ B α loss,
186 ranking in order as follows: ZnPP>PPIX>NMPP (Fig. 1F). Consistent with this NF- κ B activation,
187 RT-PCR analyses of mRNA from ZnPP-treated hepatocytes indicated marked up-regulation of
188 the inflammatory cytokine IL-6 at 24 h (Fig.1G).

189 Because p62 is a major component of MDB and various other pathological aggregates
190 [1], we monitored hepatic p62 response upon NMPP, PPIX and ZnPP \pm hemin treatments (Figs.

191 1B, 1E). In parallel with I κ B α loss, p62 formed aggregates and possibly cross-linked species,
192 with a concurrent decline in the monomeric species (~62 kD; Ctrl), evident at later (8 h) rather
193 than earlier (2-4 h) time points. This apparent time-lag is most likely due to an initial
194 counteractive compensatory p62 transcriptional induction in response to PPIX-elicited oxidative
195 stress and Nrf2 activation [8]. Furthermore, we found that the p62-monomer levels correlated
196 reasonably well ($r^2 = 0.72$) with corresponding I κ B α levels in these treated and untreated cells,
197 revealing an intimate association between I κ B α loss and p62-aggregation, possibly due to their
198 direct protein interactions (Fig. S1D).

199

200 ***ZnPP-elicited I κ B α -loss is independent of p62 or other autophagic receptors/adapters:***

201 The capacity of p62 to stabilize I κ B α upon co-expression in HEK293T cells (Fig. 2A) and the
202 close temporal relationship between I κ B α -loss and p62 aggregation (Fig. 1B) suggested these
203 proteins were intimately associated. We thus examined their interdependence in ZnPP-treated
204 p62 WT and p62 null mouse (p62KO) hepatocytes or MEF cells (Figs. 2B & S4A), and found
205 that this I κ B α loss was independent of p62 aggregation. The additional possibility that in p62-
206 lacking cells, I κ B α loss was due to its degradation via UPD, ALD or calpain pathways was
207 excluded with specific inhibitors of these pathways (Fig. S4B). We also examined plausible
208 compensation by NBR1 (Neighbour of Braca 1 gene) [34] (Fig S4C, S4D), and three other
209 autophagic receptors/adapters [35], and conclusively excluded p62 and its redundant functional
210 mimics in this ZnPP-elicited I κ B α -loss (Fig. 2D).

211

212 ***Cytoplasmic I κ B α -loss is due to its physical sequestration into insoluble cellular***

213 ***aggregates:*** Confocal microscopic immunofluorescence (CMIF) analyses of ZnPP-treated WT
214 and p62^{-/-}-MEF cells provided an informative clue (Fig. 2E). In WT-cells, both proteins were

215 largely colocalized to the cytoplasm, and ZnPP did not affect this colocalization (Fig. 2E, insets).
216 Surprisingly, following ZnPP-treatment, in spite of immunochemical I κ B α -loss (Fig. 2D), I κ B α -
217 associated immunofluorescence signal still persisted comparably in both WT and p62^{-/-}-MEF
218 cells. This finding provided the first clue that upon ZnPP-treatment, I κ B α was not irretrievably
219 lost, but just undetectable in detergent-solubilized cell lysates routinely employed for
220 immunoblotting (IB) analyses. It was thus likely that such an I κ B α physical inaccessibility was
221 due to intracellular ZnPP-triggered protein aggregation. To examine this possibility, HEK293T
222 cells co-transfected with both HA-I κ B α and p62-Myc plasmids, were treated with ZnPP and
223 then sequentially extracted using detergents of increasing strengths (Supplementary Methods).
224 IB analyses showed that upon ZnPP-treatment, in parallel with p62 aggregation, HA-
225 I κ B α became undetectable in soluble Triton and RIPA fractions (Fig. 3A), however, the majority
226 of HA-I κ B α as well as monomeric p62 and p62-aggregates could be recovered from the RIPA-
227 insoluble pellet by heat extraction with 8M urea/CHAPS buffer (urea buffer; Supplementary
228 Methods). Furthermore, similar results were found upon IB analyses of these urea extracts
229 irrespective of whether antibodies to the HA-tag, N- or C-terminus of I κ B α were employed (Fig.
230 3B). IB analyses of high salt buffer (HSB)-extracts from ZnPP-treated cell lysates also revealed
231 detectable monomeric and aggregated I κ B α and p62 species, albeit to a much lesser extent
232 than corresponding urea extracts (Fig. 3C). Together, these findings indicated that upon ZnPP-
233 treatment, p62 and I κ B α along with other cellular proteins co-aggregate, and these aggregates
234 are sequestered from the cytoplasm into an insoluble cellular fraction, essentially unavailable to
235 function physiologically.

236

237 ***Proteomic identification of plausible I κ B α -interactors and ZnPP-aggregated proteins:***

238 PPIX-treatment is causally associated with the highly selective aggregation of many cellular

239 proteins [36]. Thus, I κ B α could either be the prime target of ZnPP-elicited physical sequestration
240 or a silent partner dragged along for the ride by one or more of its cellular interactors. To identify
241 any plausible mediators of ZnPP-elicited I κ B α sequestration into insoluble cellular aggregates,
242 we employed a proteomic approach to comprehensively identify the proteins that normally
243 interact with I κ B α , but which form protein co-aggregates upon ZnPP-treatment. These
244 aggregation-prone proteins upon I κ B α -interaction could drive its sequestration and co-
245 aggregation.

246 To obtain a high-confidence I κ B α -interactome, we performed rigorous immunoaffinity
247 purification coupled with mass spectrometry (IAP-MS) analyses, with extensive biological
248 repetitions and strict filtering (Fig. 4A, 4B, Supplementary Methods). This approach identified
249 370 high-confidence I κ B α -interactors, including well-established I κ B α -interactors [i.e. NF- κ B
250 subunits (RelA, NFKB1, NFKB2), and IKK-complex proteins (CHUK, IKBKAP)] (Fig. 4C), thus
251 validating our IAP-MS approach. However, most of the proteins identified were novel I κ B α -
252 interactors.

253 Previous studies in *fech/fech* mouse and protoporphyrin zebra fish models have
254 identified several (\approx 30) aggregated proteins in the high molecular mass (HMM)-regions upon
255 SDS-PAGE of NP40-soluble and/or SDS-soluble liver fractions [8, 13, 36, 37]. Our discovery
256 that ZnPP-elicited protein aggregates could be resolubilized by heating in urea buffer, prompted
257 comprehensive proteomic analyses of these urea-solubilized protein aggregates. For this
258 purpose, the progressive temporal course of this protein aggregation process was followed in
259 HEK293T and HepG2 cells treated with ZnPP for 2 h and 24 h (Fig. 4D). The entire urea-
260 solubilized fraction as well as the HMM-bands from SDS-PAGE of Triton and RIPA soluble
261 extracts were subjected to LC-MS/MS proteomic analyses (Fig. 4D, E). Overlap analyses

262 revealed that 192 proteins commonly aggregated in both cell lines upon ZnPP-treatment (Fig.
263 4F).

264

265 ***Disruption of multiple functional networks upon ZnPP-elicited physical sequestration of***

266 ***I κ B α and other cellular proteins:*** To gain functional insight into these 192 ZnPP-aggregated

267 proteins and their possible contribution to cell toxicity, we undertook a comprehensive protein

268 network analyses using the Search Tool for the Retrieval of Interacting Genes/Proteins

269 (STRING) coupled with biological process and pathway overrepresentation analyses (Fig. 5A).

270 Clearly, ZnPP-elicited physical aggregation clustered these proteins under 4 critical biological

271 processes. Those proteins occupying a network hub/node position within their individual clusters,

272 could disrupt multiple vital cellular interactions, leading to global hepatic functional collapse.

273 Additional overlap of the 370 I κ B α -interacting proteome with the common 192 ZnPP-aggregate

274 proteome identified 47 I κ B α -interacting proteins in common with the ZnPP-aggregate proteome

275 (*each highlighted in yellow*; Fig. 5A). By contrast, well-established I κ B α interactors (RelA,

276 NFKB1, NFKB2, CHUK and IKBKAP) were not detected within the ZnPP-aggregate proteome of

277 either cell type (Fig. 5A). An enrichment ratio of the 47 overlapping proteins under each

278 experimental condition was then employed to percentile rank them in a heat-map clustering

279 format (Fig. 5B). Such analyses identified many nuclear pore complex (NPC) nucleoporins

280 Nup153, Nup155, and Nup93, and Nup358/SUMO E3-ligase RANBP2, as significantly enriched

281 in this combined proteome (Fig. 5B).

282 To further verify that these 47 proteins were indeed co-aggregating with I κ B α , rather

283 than merely aggregating in parallel, we employed biotinylation proximity labeling to identify

284 I κ B α -interacting proteins within the protein aggregates. After due consideration of various

285 proximity labeling approaches, we selected HRP-biotinylation by antibody recognition (BAR) [38]

286 for identification of I κ B α -interacting proteins in both soluble and insoluble fractions of ZnPP-
287 treated and untreated cells (Fig. S5). The overlapping proteome identified via both co-IP and
288 BAR approaches revealed a very high-confidence I κ B α -interactome. More importantly, of the
289 previously identified 47 I κ B α -interacting proteins in common with the ZnPP-aggregate proteome,
290 37 were also detected via BAR to be interacting with I κ B α in ZnPP-triggered protein aggregates
291 (Fig 5B), indicating that they were indeed co-aggregating.

292

293 ***Nucleoporin Nup153 is a principal I κ B α -interactant and ZnPP-target:*** The heat-map
294 clustering analyses of these 47 proteins consistently identified the nuclear pore basket
295 component Nup153 as the top common I κ B α -interactant in IAP-MS, BAR, and HEK293 and
296 HepG2 ZnPP-aggregate proteome. We therefore verified Nup153 presence through IB analyses
297 of Triton- and urea-solubilized cellular aggregates upon a 2 h-ZnPP-treatment of HEK293 and
298 HepG2 cells. Indeed, whereas native Nup153 exhibited its intrinsic 153 kDa-mobility in
299 untreated cells, upon ZnPP-treatment it was found as HMM-protein aggregates in Triton- and
300 urea extracts, along with endogenous I κ B α (Fig. 6A). Furthermore, co-immunoprecipitation (Co-
301 IP) using HEK293T cells revealed a significant fraction of endogenous Nup153 interacted with
302 I κ B α both in cytoplasmic and nuclear extracts of GFP-I κ B α -transfected cells, but not in mock- or
303 C1-GFP-transfected cells (Fig. 6B). A similar interaction was also evident among the
304 endogenous counterparts under basal conditions. However, this Nup153-I κ B α -interaction was
305 greatly enhanced upon TNF α -treatment at times (1 and 1.5 h) when rapid translocation of *de*
306 *nov* synthesized I κ B α across the nuclear pore would be expected to trigger its post-induction
307 repression of NF- κ B-activation (Fig. 6C). Furthermore, ZnPP-treatment of TNF α -pretreated cells
308 led to accelerated I κ B α sequestration, whose timing revealed that ZnPP may preferentially
309 target *de novo* synthesized I κ B α as it increasingly interacts with cytoplasmic Nup153 during its

310 nuclear import (Fig. 6C-D). Consistent with this, our CMIF of HepG2 cells revealed that under
311 basal conditions, both NF- κ B (p65-Rel A subunit) and I κ B α are localized in the cytoplasm (Fig.
312 6E). But upon TNF α -treatment, I κ B α UPD results in NF- κ B nuclear translocation within 0.5 h.
313 Subsequently, upon transcriptional activation of the NF- κ B-responsive I κ B α -gene, newly
314 synthesized I κ B α enters the nucleus resulting in NF- κ B dissociation and nuclear export, all
315 within 1 h of TNF α -treatment. By contrast, upon ZnPP-treatment, in spite of this robust I κ B α -
316 restoration at 1 h after TNF α -treatment, it is apparently functionally defective as a nuclear NF-
317 κ B-repressor, as NF- κ B persisted in the nucleus (Fig. 6E). This stalled I κ B α appears
318 prominently both in the cytoplasm as well as clustered around the outer nuclear envelope rim
319 (Fig. 6E). Additional support for this likelihood is provided by our Nup153 and RanBP2 siRNA-
320 knockdown analyses that revealed the marked attenuation of nuclear I κ B α -import upon TNF α -
321 activation, without affecting its ZnPP-sequestration (Figs. 7 & S6).

322

323 ***I κ B α siRNA knockdown analyses reveal that ZnPP-triggered NF- κ B activation may***
324 ***additionally involve I κ B β -sequestration:*** Because of the functional redundancy of various
325 I κ Bs in NF- κ B cytoplasmic retention, I κ B α -deficiency through genetic ablation, siRNA
326 knockdown, or cycloheximide-inhibition of I κ B α -synthesis fails to increase constitutive NF- κ B
327 transcriptional activation in many nonhepatic cell-types [19, 39, 40]. Thus, upon our I κ B α
328 siRNA-knockdown, a similar slight, barely detectable constitutive NF- κ B activation was
329 observed in HepG2 cells (Fig. 8A, left panel), whereas in primary mouse hepatocytes this
330 activation was quite substantial (Fig. 8A, right panel). However, it was not quite as marked as
331 that observed upon ZnPP-treatment, possibly due to the significant compensatory I κ B β -
332 upregulation upon I κ B α siRNA-knockdown (Fig. 8B). Because in hepatocytes both I κ B α and
333 I κ B β are the predominantly expressed I κ Bs [18, 21], and given the relatively more pronounced,

334 sustained and consistently reproducible ZnPP-elicited NF- κ B activation, we determined whether
335 ZnPP also similarly sequestered I κ B β . Indeed, upon I κ B α siRNA of HepG2 cells, the
336 compensatorily increased I κ B β was similarly targeted to ZnPP-elicited aggregation, resulting in
337 no appreciable mitigation of the ZnPP-induced NF- κ B activation post I κ B α -knockdown (Fig 8C).
338 Furthermore, immunoblotting re-analyses of the RIPA-soluble ZnPP-treated lysates revealed
339 that I κ B β also disappeared from its usual monomeric position, but was found in HMM protein
340 aggregates (Fig. 8D). Such an apparent “I κ B β -loss” was also resistant to various UPD, calpain
341 and ALD inhibitors, consistent with a sequestration process similar to that of I κ B α . The ZnPP-
342 targeting of both hepatic I κ Bs thus accounts for its potent NF- κ B activation. Accordingly, *in vivo*
343 ZnPP-treatment of mice revealed marked mRNA increases of several hepatic proinflammatory
344 NF- κ B target genes i.e. IL-6, IL-1 β , TNF α and osteopontin (Fig. 8D)

345

346 DISCUSSION

347 ***Why is I κ B α vulnerable to ZnPP-elicited physical sequestration from the cytoplasm?***

348 Recent evidence increasingly supports a sequestration and co-aggregation model of
349 pathogenesis [41]. In a snowballing effect, aggregation-prone disease proteins “hijack” their
350 interacting partners with vital functions, sequestering them into cytotoxic insoluble inclusions
351 [41]. The protein scaffold p62 is one such I κ B α -co-aggregating protein. However, scrutiny of
352 ZnPP-treated p62^{-/-} hepatocytes and MEF cells reveals that it is not essential for ZnPP-elicited
353 I κ B α -sequestration. This is consistent with the report that in p62^{-/-} mouse liver, p62 is not
354 required for MDB formation, just for their maturation and stability [42]. These aggregation-prone
355 proteins share some common physicochemical properties: Preexistent proteins are relatively
356 large in size, enriched in domains with high intrinsic disorder or unstructured regions, and exhibit
357 low average hydrophobicity [43]; newly synthesized proteins on the other hand, are more

358 vulnerable due to prolonged exposure of their relatively hydrophobic domains either during or
359 soon after synthesis during their subsequent folding, assembly, or transport [43].

360 None of the 47 proteins that interacted with I κ B α and co-aggregated upon ZnPP-
361 treatment is a well-established stable I κ B α interactor. Although most of the known stable I κ B α
362 interactors were repeatedly found in our co-IP analyses (Fig 4C), they were never detected in
363 the ZnPP-aggregate proteome. This suggests that these 47 proteins may be transient
364 I κ B α interactors that are difficult to capture without highly sensitive and selective approaches.
365 Our analyses of the physicochemical properties of these 47 proteins indicated that they ranged
366 widely in size, with ~90% exhibiting relatively low hydrophobicity, and ~80% predicted to contain
367 a long (>30 residues) disordered segment (Table S1). These dual features of low hydrophobicity
368 coupled with high intrinsic disorder could synergistically contribute to their ZnPP-elicited co-
369 aggregation upon transient interaction, and may explain why ZnPP initially targets preexistent
370 I κ B α species exhibiting both features (Table S1). The structurally related I κ B β is similarly
371 vulnerable to ZnPP-elicited sequestration thus accounting for the remarkably profound NF- κ B-
372 activation. Whether this vulnerability stems from their common structural ankyrin-repeat domain
373 feature remains to be determined. Free I κ B α species is apparently unstable and requires NF- κ B
374 binding for folding to a stable conformation [44]. After TNF α stimulation, newly synthesized
375 I κ B α would be unstable and thus greatly susceptible to ZnPP-elicited aggregation without
376 nuclear import in order to bind NF- κ B and properly fold, thus resulting in the sustained ZnPP-
377 triggered NF- κ B-activation.

378 Although NF- κ B and I κ B α form a stable complex, they are not static cytoplasmic
379 residents but shuttle continuously between the nucleus and cytoplasm [45]. Interestingly, p65
380 and I κ B α translocate into the nucleus via different pathways. p65 enters the nucleus via the
381 classical NLS-and importin (α 3/ α 4)-dependent machinery [46], whereas I κ B α and several other

382 ankyrin repeat domain-containing proteins (ARPs) enter the nucleus via a NLS- and importin-
383 *independent* machinery [47]. This machinery depends on a direct interaction between the ARPs,
384 RanGDP as well as mobile nucleoporins such as Nup153 and RanBP2 for entry across the NPC
385 into the nucleus. Indeed, plausibly relevant to this $\text{I}\kappa\text{B}\alpha$ -nucleocytoplasmic shuttling process, our
386 proteomic analyses of the 47 common $\text{I}\kappa\text{B}\alpha$ -interacting and ZnPP-co-aggregating proteins
387 underscored significant enrichment of mobile NPC nucleoporins. Of these, our heat-map
388 analyses singled out Nup153 as both the top-ranked $\text{I}\kappa\text{B}\alpha$ -interactant and ZnPP-aggregation
389 target (Fig. 5B). By contrast, importins $\alpha 3$ and $\alpha 4$ relevant to p65 nuclear import were not found
390 in the ZnPP-aggregate proteome, which may explain why p65 is not co-aggregated during its
391 nuclear import.

392

393 **Potential role of Nup153 in $\text{I}\kappa\text{B}\alpha$ -mediated NF- κB -repression:** The nucleoporin Nup153
394 primarily exists N-terminally anchored to the nuclear pore basket while its disordered and
395 flexible FG-rich C-terminus extends into the cytoplasm [48]. Another Nup153 pool apparently
396 exists that shuttles between the cytoplasmic and NPC faces [49], and interacts directly with
397 cargos (i.e. Stat1, Smad2, and PU.1) for their nuclear import via a transporter-*independent*
398 machinery [48]. Nup153, in contrast to other FG-rich nucleoporins i.e. Nup98, Nup62, Nup214,
399 also strongly binds ARs of iASPP and ASPP2, two representative substrates of the NLS-
400 independent ARP-RanGDP nuclear import pathway [47]. Structural/biochemical analyses
401 indicate that Nup153 binds RanGDP at a higher affinity than RanGTP [50]. This collective
402 evidence suggests a critical role of Nup153 in facilitating ARP-RanGDP nuclear import. Our
403 findings that $\text{I}\kappa\text{B}\alpha$ co-immunoprecipitated not only with Nup153 in the nuclear extracts (NER),
404 but also more appreciably with that in the cytoplasmic extracts (CER), even though the basal
405 cytoplasmic Nup153-content is much lower than its nuclear content (compare inputs, Fig. 6B),

406 are consistent with a minor, albeit highly dynamic, cytoplasmic Nup153 pool. This pool directly
407 interacts with I κ B α and may be responsible for the continuous I κ B α -nucleocytoplasmic traffic at
408 steady state, as indeed verified by our Nup153 knockdown analyses (Fig. 7). The concurrent
409 ZnPP-elicited aggregation of Nup153 and I κ B α suggests that the basal nuclear import of
410 I κ B α as well as that of newly synthesized I κ B α after TNF α -stimulation is disrupted, leading to
411 NF- κ B nuclear persistence and prolonged response.

412 Another noteworthy proteomic finding is our quite prominent detection of the SUMO E3-
413 ligase RanBP2 in this 47-protein cohort. RanBP2, an outer NPC component, fans its FG-rich
414 filaments into the cytoplasm [51]. The proteomic detection of RanBP2, but no other cytoplasmic
415 NPC nucleoporin i.e. Nup214 in this common 47-protein cohort is functionally intriguing because
416 besides Nup153, RanBP2 is also involved in receptor-independent nuclear import through direct
417 interactions with its specific cytoplasmic cargos [51]. This is intriguing given that I κ B α
418 SUMOylation is reportedly involved in its nuclear entry and subsequent post-induction NF- κ B-
419 repression [52]. Because RanBP2 also strongly binds RanGDP, conceivably a RanBP2-
420 RanGDP-Nup153-I κ B α -SUMO complex is involved in I κ B α -nuclear import, a possibility
421 consistent with our RanBP2 knockdown analyses (Fig. 7). The inviability of actively dividing
422 HEK293T cells precluded our simultaneous knockdown of both nucleoporins to mimic their
423 concurrent ZnPP-elicited sequestration. The failure of Nup153 or RanBP2 knockdown to affect
424 ZnPP-elicited I κ B α -sequestration suggests that the newly synthesized I κ B α is itself vulnerable,
425 particularly in the absence of both Nup153 and RanBP2 to chaperone its nuclear entry.

426 We find it quite instructive that many of these nucleocytoplasmic trafficking proteins as
427 well as others within the 47 co-aggregated proteome are well-established components of
428 pathogenic neurodegenerative disease protein aggregates (MS and ALS) or inclusions
429 (Parkinson's Lewy bodies), as well as hepatic MDBs (liver disease and hepatic protoporphyria

430 models) [Fig. 5B; [13, 36, 37, 43, 53, 54]]. For example, Nup153 was shown not only to co-
431 aggregate with cargo proteins in oligodendrocyte precursor cells in MS lesions [55], but also
432 detected as anterior horn cell cytoplasmic inclusions of an ADAR2-deficient ALS mouse model
433 [56]. These findings not only underscore the common intrinsic physicochemical and
434 physiological properties of these aggregation-prone proteins, but also suggest that their
435 interaction with $\text{I}\kappa\text{B}\alpha$ could also similarly drive their co-aggregation under disease stresses, and
436 thus account for the associated tissue inflammation and injury commonly seen in both liver and
437 neurodegenerative diseases.

438

439 ***Plausible clinical relevance to EPP and XLPP:*** Such ZnPP-elicited persistent NF- κ B
440 transcriptional activation may also account for the inflammation and injury stemming from
441 chronic PPIX exposure not only in $\text{Fech}^{\text{m1Pas}}$, DDC- and GF-protoporphyrin rodent livers, but
442 also in EPP and XLPP patient livers [10, 11, 28-30, 57], wherein avid Fe-overutilization may
443 drive ZnPP-generation. ZnPP generation is also a prominent feature of iron-deficiency anemias
444 and lead poisoning (Lamola and Yamane, 1974), Although our studies were largely confined to
445 primary hepatocytes, in intact protoporphyrin human and mouse livers these parenchymal cells
446 are juxtaposed to non-parenchymal Kupffer cells and hepatic stellate cells that are quite capable
447 of both canonical and non-canonical NF- κ B-signaling. Thus, upon chronic PPIX-exposure, their
448 NF- κ B-activation could induce proinflammatory cytokines, chemokines, growth factors and other
449 mitogens [17]. This additional paracrine cytokine stimulus could further potentiate the PPIX-
450 elicited NF- κ B-signaling activation within the hepatocyte, further aggravating the extent of EPP
451 and XLPP liver injury. Indeed, exogenous $\text{TNF}\alpha$ greatly accelerated ZnPP-elicited $\text{I}\kappa\text{B}\alpha$ -
452 sequestration in hepatocytes (Fig. 6D)

453 The precise mechanism of PPIX-induced protein aggregation remains to be elucidated.
454 Porphyrins trigger protein cross-linking through a secondary reaction between the
455 photooxidative products of histidine, tyrosine and/or tryptophan and free NH₂-groups of amino
456 acids [58]. Given the light-sheltered *in vivo* environment of the liver, such a photooxidative
457 protein crosslinking seems unlikely in PPIX-mediated hepatic MDB formation, although PPIX
458 can trigger protein aggregation and cell toxicity in the dark, albeit at a slower rate [36].
459 Additionally, porphyrins also induce structural changes in certain proteins, leading to their
460 functional impairment [59]. Such structural changes could expose some hydrophobic regions
461 thereby inducing protein aggregation. In this context, the 192 PPIX-targeted aggregate proteins
462 identified herein, we propose, could provide valuable insight into the future elucidation of the
463 precise mechanism of PPIX-induced protein aggregation.

464

465 **Experimental Procedures**

466 **Cell culture and transfections**

467 Primary mouse hepatocytes were isolated from C57BL/6 wild type male mice by collagenase
468 perfusion. HepG2, HeLa, HEK293T and MEF cells were cultured using standard methods.
469 HEK293T cells were transfected using TurboFect (ThermoFisher) and HepG2 cells were
470 transfected using X-tremeGENE HP (Roche) according to the manufacturers' instructions. See
471 Extended Experimental Procedures for details.

472

473 **EMSA**

474 Nuclear fractions of cells were prepared using NE-PER Nuclear and Cytoplasmic Extraction
475 Reagents (ThermoFisher). EMSA were performed using LightShift Chemiluminescent EMSA Kit
476 (ThermoFisher). See Extended Experimental Procedures for details.

477

478 **Western Immunoblotting (IB) Analyses:**

479 Whole-cell extracts were prepared with Cell Lysis buffer (Cell Signaling Technology)
480 supplemented with 10% glycerol and protease/phosphatase inhibitor cocktail (Pierce). Cell
481 lysates were sonicated for 10s and then cleared by centrifugation at 4°C in a tabletop centrifuge
482 at the highest speed for 10 min. Protein concentrations were determined by BCA assay and
483 equal amounts of proteins were separated on Tris-Glycine eXtended (TGX) polyacrylamide gels.
484 Proteins were transferred onto nitrocellulose membranes (Biorad, Hercules, CA) for IB analyses.
485 See Extended Experimental Procedures for details.

486

487 **Mass spectrometry (MS):**

488 Samples subject to MS proteomics analyses were processed using standard in-gel digestion
489 and the resulting peptide mixture was desalted using C18-Ziptips (Millipore) and then injected
490 into an LTQ-Orbitrap Velos mass spectrometer (Thermo Fisher). Raw data were processed
491 using ProteinProspector (version 5.19.1; <http://prospector.ucsf.edu/prospector/mshome.htm>).
492 See Extended Experimental Procedures for details.

493

494

495 **Acknowledgments:** We gratefully acknowledge Mr. Chris Her, UCSF Liver Cell & Tissue
496 Biology Core Facility (supported by NIDDK Grant P30DK26743) for hepatocyte isolation. We are
497 most grateful to Dr. D. M. Bissell (UCSF) for valuable discussions and his critical review of our
498 manuscript. We also gratefully acknowledge Prof. P. Ortiz de Montellano (UCSF) for valuable
499 discussions of porphyrin chemistry, and Dr. G. Knudsen (UCSF) for her helpful comments on
500 our IAP/MS methodology and critical review of our manuscript and proteomic data. We also
501 sincerely thank Profs. T. Ishii, M. Komatsu, H. Zhu, N. Mizushima, R. Scheckman, and R. J.
502 Youle for valuable cell-lines. Y. Liu is most grateful to Dr. D. Larsen, UCSF Nikon Imaging
503 Center for her training in confocal immunofluorescence microscopy, and Drs. M. Laurance,
504 UCSF HDF Comprehensive Cancer Center and A. Pico, The Gladstone Institute Bioinformatics
505 Facility, for training on pathway analyses and visualization.

506

507

508 **References:**

- 509 [1] Strnad P, Zatloukal K, Stumptner C, Kulaksiz H, Denk H. Mallory-Denk-bodies: lessons
510 from keratin-containing hepatic inclusion bodies. *Biochim Biophys Acta* 2008;1782:764-774.
- 511 [2] Zatloukal K, Stumptner C, Fuchsbichler A, Heid H, Schnoelzer M, Kenner L, et al. p62 Is
512 a common component of cytoplasmic inclusions in protein aggregation diseases. *Am J Pathol*
513 2002;160:255-263.
- 514 [3] Jensen K, Gluud C. The Mallory body: morphological, clinical and experimental studies
515 (Part 1 of a literature survey). *Hepatology* 1994;20:1061-1077.
- 516 [4] Denk H, Gschnait F, Wolff K. Hepatocellular hyalin (Mallory bodies) in long term
517 griseofulvin-treated mice: a new experimental model for the study of hyalin formation. *Lab Invest*
518 1975;32:773-776.
- 519 [5] Yokoo H, Harwood TR, Racker D, Arak S. Experimental production of Mallory bodies in
520 mice by diet containing 3,5-diethoxycarbonyl-1,4-dihydrocollidine. *Gastroenterology*
521 1982;83:109-113.
- 522 [6] Holley AE, Frater Y, Gibbs AH, De Matteis F, Lamb JH, Farmer PB, et al. Isolation of two
523 N-monosubstituted protoporphyrins, bearing either the whole drug or a methyl group on the
524 pyrrole nitrogen atom, from liver of mice given griseofulvin. *Biochem J* 1991;274 (Pt 3):843-848.
- 525 [7] Ortiz de Montellano PR, Beilan HS, Kunze KL. N-Alkylprotoporphyrin IX formation in 3,5-
526 dicarboxy-1,4-dihydrocollidine-treated rats. Transfer of the alkyl group from the substrate to
527 the porphyrin. *J Biol Chem* 1981;256:6708-6713.
- 528 [8] Singla A, Moons DS, Snider NT, Wagenmaker ER, Jayasundera VB, Omary MB.
529 Oxidative stress, Nrf2 and keratin up-regulation associate with Mallory-Denk body formation in
530 mouse erythropoietic protoporphyria. *Hepatology* 2012;56:322-331.
- 531 [9] Schiff ER, Maddrey WC, Sorrell MF. Hepatic Histopathology. *Schiff's Diseases of the*
532 *Liver: Wiley; 2011. p. 280-282.*
- 533 [10] Davies R, Schuurman A, Barker CR, Clothier B, Chernova T, Higginson FM, et al.
534 Hepatic gene expression in protoporphyric Fech mice is associated with cholestatic injury but not
535 a marked depletion of the heme regulatory pool. *Am J Pathol* 2005;166:1041-1053.
- 536 [11] Gant TW, Baus PR, Clothier B, Riley J, Davies R, Judah DJ, et al. Gene expression
537 profiles associated with inflammation, fibrosis, and cholestasis in mouse liver after griseofulvin.
538 *EHP Toxicogenomics* 2003;111:37-43.
- 539 [12] Stumptner C, Fuchsbichler A, Heid H, Zatloukal K, Denk H. Mallory body--a disease-
540 associated type of sequestosome. *Hepatology* 2002;35:1053-1062.
- 541 [13] Singla A, Griggs NW, Kwan R, Snider NT, Maitra D, Ernst SA, et al. Lamin aggregation
542 is an early sensor of porphyria-induced liver injury. *J Cell Sci* 2013;126:3105-3112.
- 543 [14] Currais A, Fischer W, Maher P, Schubert D. Intraneuronal protein aggregation as a
544 trigger for inflammation and neurodegeneration in the aging brain. *FASEB J* 2017;31:5-10.
- 545 [15] Nivon M, Fort L, Muller P, Richet E, Simon S, Guey B, et al. NFkappaB is a central
546 regulator of protein quality control in response to protein aggregation stresses via autophagy
547 modulation. *Mol Biol Cell* 2016;27:1712-1727.
- 548 [16] Liou HC, Baltimore D. Regulation of the NF-kappa B/rel transcription factor and I kappa
549 B inhibitor system. *Curr Opin Cell Biol* 1993;5:477-487.
- 550 [17] He G, Karin M. NF-kappaB and STAT3 - key players in liver inflammation and cancer.
551 *Cell Res* 2011;21:159-168.
- 552 [18] Azimifar SB, Nagaraj N, Cox J, Mann M. Cell-type-resolved quantitative proteomics of
553 murine liver. *Cell Metab* 2014;20:1076-1087.
- 554 [19] Han Y, Brasier AR. Mechanism for biphasic rel A. NF-kappaB1 nuclear translocation in
555 tumor necrosis factor alpha-stimulated hepatocytes. *J Biol Chem* 1997;272:9825-9832.

- 556 [20] Rao P, Hayden MS, Long M, Scott ML, West AP, Zhang D, et al. IkappaBbeta acts to
557 inhibit and activate gene expression during the inflammatory response. *Nature* 2010;466:1115-
558 1119.
- 559 [21] Wisniewski JR, Vildhede A, Noren A, Artursson P. In-depth quantitative analysis and
560 comparison of the human hepatocyte and hepatoma cell line HepG2 proteomes. *J Proteomics*
561 2016;136:234-247.
- 562 [22] Beg AA, Finco TS, Nantermet PV, Baldwin AS, Jr. Tumor necrosis factor and interleukin-
563 1 lead to phosphorylation and loss of I kappa B alpha: a mechanism for NF-kappa B activation.
564 *Mol Cell Biol* 1993;13:3301-3310.
- 565 [23] Traenckner EB, Wilk S, Baeuerle PA. A proteasome inhibitor prevents activation of NF-
566 kappa B and stabilizes a newly phosphorylated form of I kappa B-alpha that is still bound to NF-
567 kappa B. *EMBO J* 1994;13:5433-5441.
- 568 [24] Weil R, Laurent-Winter C, Israel A. Regulation of IkappaBbeta degradation. Similarities
569 to and differences from IkappaBalpha. *J Biol Chem* 1997;272:9942-9949.
- 570 [25] Arenzana-Seisdedos F, Thompson J, Rodriguez MS, Bachelier F, Thomas D, Hay RT.
571 Inducible nuclear expression of newly synthesized I kappa B alpha negatively regulates DNA-
572 binding and transcriptional activities of NF-kappa B. *Mol Cell Biol* 1995;15:2689-2696.
- 573 [26] Thompson JE, Phillips RJ, Erdjument-Bromage H, Tempst P, Ghosh S. I kappa B-beta
574 regulates the persistent response in a biphasic activation of NF-kappa B. *Cell* 1995;80:573-582.
- 575 [27] Arenzana-Seisdedos F, Turpin P, Rodriguez M, Thomas D, Hay RT, Virelizier JL, et al.
576 Nuclear localization of I kappa B alpha promotes active transport of NF-kappa B from the
577 nucleus to the cytoplasm. *J Cell Sci* 1997;110 (Pt 3):369-378.
- 578 [28] Cox TM. Protoporphyrin. In: Karl M. Kadish KMS, Roger Guilard, editor. *The Porphyrin*
579 *Handbook: Medical aspects of porphyrins*. USA: Elsevier science; 2003.
- 580 [29] Thapar M, Bonkovsky HL. The diagnosis and management of erythropoietic
581 protoporphyria. *Gastroenterol Hepatol (N Y)* 2008;4:561-566.
- 582 [30] Balwani M, Doheny D, Bishop DF, Nazarenko I, Yasuda M, Dailey HA, et al. Loss-of-
583 function ferrochelatase and gain-of-function erythroid-specific 5-aminolevulinate synthase
584 mutations causing erythropoietic protoporphyria and x-linked protoporphyria in North American
585 patients reveal novel mutations and a high prevalence of X-linked protoporphyria. *Mol Med*
586 2013;19:26-35.
- 587 [31] Chen JJ. Regulation of protein synthesis by the heme-regulated eIF2alpha kinase:
588 relevance to anemias. *Blood* 2007;109:2693-2699.
- 589 [32] Cuervo AM, Hu W, Lim B, Dice JF. IkappaB is a substrate for a selective pathway of
590 lysosomal proteolysis. *Mol Biol Cell* 1998;9:1995-2010.
- 591 [33] Chen F, Lu Y, Kuhn DC, Maki M, Shi X, Sun SC, et al. Calpain contributes to silica-
592 induced I kappa B-alpha degradation and nuclear factor-kappa B activation. *Arch Biochem*
593 *Biophys* 1997;342:383-388.
- 594 [34] Kirkin V, Lamark T, Sou YS, Bjorkoy G, Nunn JL, Bruun JA, et al. A role for NBR1 in
595 autophagosomal degradation of ubiquitinated substrates. *Mol Cell* 2009;33:505-516.
- 596 [35] Lazarou M, Sliter DA, Kane LA, Sarraf SA, Wang C, Burman JL, et al. The ubiquitin
597 kinase PINK1 recruits autophagy receptors to induce mitophagy. *Nature* 2015;524:309-314.
- 598 [36] Maitra D, Elenbaas JS, Whitesall SE, Basur V, D'Alecy LG, Omary MB. Ambient Light
599 Promotes Selective Subcellular Proteotoxicity after Endogenous and Exogenous
600 Porphyrinogenic Stress. *J Biol Chem* 2015;290:23711-23724.
- 601 [37] Elenbaas JS, Maitra D, Liu Y, Lentz SI, Nelson B, Hoenerhoff MJ, et al. A precursor-
602 inducible zebrafish model of acute protoporphyria with hepatic protein aggregation and
603 multiorganellar stress. *FASEB J* 2016;30:1798-1810.

- 604 [38] Bar DZ, Atkatsch K, Tavarez U, Erdos MR, Gruenbaum Y, Collins FS. Biotinylation by
605 antibody recognition-a method for proximity labeling. *Nat Methods* 2018;15:127-133.
- 606 [39] Klement JF, Rice NR, Car BD, Abbondanzo SJ, Powers GD, Bhatt PH, et al.
607 IkappaBalpha deficiency results in a sustained NF-kappaB response and severe widespread
608 dermatitis in mice. *Mol Cell Biol* 1996;16:2341-2349.
- 609 [40] Tergaonkar V, Correa RG, Ikawa M, Verma IM. Distinct roles of IkappaB proteins in
610 regulating constitutive NF-kappaB activity. *Nat Cell Biol* 2005;7:921-923.
- 611 [41] Yang H, Hu HY. Sequestration of cellular interacting partners by protein aggregates:
612 implication in a loss-of-function pathology. *FEBS J* 2016;283:3705-3717.
- 613 [42] Lahiri P, Schmidt V, Smole C, Kufferath I, Denk H, Strnad P, et al. p62/Sequestosome-1
614 Is Indispensable for Maturation and Stabilization of Mallory-Denk Bodies. *PLoS One*
615 2016;11:e0161083.
- 616 [43] Olzscha H, Schermann SM, Woerner AC, Pinkert S, Hecht MH, Tartaglia GG, et al.
617 Amyloid-like aggregates sequester numerous metastable proteins with essential cellular
618 functions. *Cell* 2011;144:67-78.
- 619 [44] Ferreira DU, Komives EA. Molecular mechanisms of system control of NF-kappaB
620 signaling by IkappaBalpha. *Biochemistry* 2010;49:1560-1567.
- 621 [45] Ghosh S, Karin M. Missing pieces in the NF-kappaB puzzle. *Cell* 2002;109 Suppl:S81-96.
- 622 [46] Fagerlund R, Kinnunen L, Kohler M, Julkunen I, Melen K. NF- κ B is transported
623 into the nucleus by importin α 3 and importin α 4. *J Biol Chem* 2005;280:15942-15951.
- 624 [47] Lu M, Zak J, Chen S, Sanchez-Pulido L, Severson DT, Endicott J, et al. A code for
625 RanGDP binding in ankyrin repeats defines a nuclear import pathway. *Cell* 2014;157:1130-1145.
- 626 [48] Ball JR, Ullman KS. Versatility at the nuclear pore complex: lessons learned from the
627 nucleoporin Nup153. *Chromosoma* 2005;114:319-330.
- 628 [49] Nakielny S, Shaikh S, Burke B, Dreyfuss G. Nup153 is an M9-containing mobile
629 nucleoporin with a novel Ran-binding domain. *EMBO J* 1999;18:1982-1995.
- 630 [50] Partridge JR, Schwartz TU. Crystallographic and biochemical analysis of the Ran-
631 binding zinc finger domain. *J Mol Biol* 2009;391:375-389.
- 632 [51] Walde S, Thakar K, Hutten S, Spillner C, Nath A, Rothbauer U, et al. The nucleoporin
633 Nup358/RanBP2 promotes nuclear import in a cargo- and transport receptor-specific manner.
634 *Traffic* 2012;13:218-233.
- 635 [52] Desterro JM, Rodriguez MS, Hay RT. SUMO-1 modification of IkappaBalpha inhibits NF-
636 kappaB activation. *Mol Cell* 1998;2:233-239.
- 637 [53] Ofengeim D, Ito Y, Najafov A, Zhang Y, Shan B, DeWitt JP, et al. Activation of
638 necroptosis in multiple sclerosis. *Cell Rep* 2015;10:1836-1849.
- 639 [54] Boeynaems S, Bogaert E, Van Damme P, Van Den Bosch L. Inside out: the role of
640 nucleocytoplasmic transport in ALS and FTLD. *Acta Neuropathol* 2016;132:159-173.
- 641 [55] Nakahara J, Kanekura K, Nawa M, Aiso S, Suzuki N. Abnormal expression of TIP30 and
642 arrested nucleocytoplasmic transport within oligodendrocyte precursor cells in multiple sclerosis.
643 *J Clin Invest* 2009;119:169-181.
- 644 [56] Yamashita T, Aizawa H, Teramoto S, Akamatsu M, Kwak S. Calpain-dependent
645 disruption of nucleo-cytoplasmic transport in ALS motor neurons. *Sci Rep* 2017;7:39994.
- 646 [57] Tutois S, Montagutelli X, Da Silva V, Jouault H, Rouyer-Fessard P, Leroy-Viard K, et al.
647 Erythropoietic protoporphyria in the house mouse. A recessive inherited ferrochelatase
648 deficiency with anemia, photosensitivity, and liver disease. *J Clin Invest* 1991;88:1730-1736.
- 649 [58] Dubbelman TM, de Goeij AF, van Steveninck J. Photodynamic effects of protoporphyrin
650 on human erythrocytes. Nature of the cross-linking of membrane proteins. *Biochim Biophys Acta*
651 1978;511:141-151.

652 [59] Afonso SG, Enriquez de Salamanca R, Batlle AM. The photodynamic and non-
653 photodynamic actions of porphyrins. *Braz J Med Biol Res* 1999;32:255-266.

654
655

656

657 **FIGURE LEGENDS:**

658 ***FIGURE 1. NMPP treatment results in concurrent PPIX-accumulation, NF- κ B activation***

659 ***and I κ B α -loss.*** **A.** A scheme for NMPP-mediated inhibition of ferrochelatase with consequent

660 accumulation of the heme precursor PPIX. The PPIX content of lysates from mouse

661 hepatocytes treated with two different commercial lots of NMPP for 24 h quantified

662 flurometrically (Mean \pm SD, n = 3). **B.** IB analyses of p62 and I κ B α with histone H3 as the

663 loading control in lysates from mouse hepatocytes treated as indicated. NMPP (30 μ M), hemin

664 (10 μ M added fresh every 4 h), and ALIs, autophagy/lysosomal inhibitors 3MA (5 mM) + NH₄Cl

665 (30 mM), and MG132 (20 μ M) for 1 h. **C.** Mouse hepatocytes were treated as indicated.

666 Representative EMSA of nuclear extracts (NER, 5 μ g) with NF- κ B-specific oligonucleotides is

667 shown. Bar chart represents mean \pm SD of NF- κ B activation relative to controls, n = 3. **D.**

668 Quantification of I κ B α levels upon IB analyses of lysates from wild type (WT) and HRI^{-/-} mouse

669 hepatocytes treated with 30 μ M NMPP for the indicated times (Mean \pm SD, n = 3). **E.** IB

670 analyses of p62 and I κ B α in lysates from mouse hepatocytes treated with 10 μ M PPIX, 10 μ M

671 ZnPP or 30 μ M NMPP with or without 10 μ M hemin for 8 h. NS, non-specific band. **F.** EMSA of

672 nuclear extracts (NER) from mouse hepatocytes treated as indicated for 24 h. **G.** IL-6 RT-PCR

673 analyses of mRNA from mouse hepatocytes treated with 10 μ M ZnPP for the indicated times

674 (Mean \pm SD, n = 3).

675

676 ***FIGURE 2. ZnPP-elicited I κ B α -loss is p62-independent.*** **A.** HEK293T cells were transfected

677 with pCMV4-3HA-I κ B α , or co-transfected with either pcDNA6-p62-Myc or pcDNA6-Myc empty

678 vector for 48 h. Cell lysates were used for IB analyses with actin as the loading control. **B.**
679 Primary hepatocytes from wild type (p62WT) and p62 knockout (p62KO) mice were treated with
680 10 μ M ZnPP for the indicated times. Cell lysates were used for IB analyses. **C.** Wild-type Hela
681 cells (WT) and CRISPR-engineered Hela cells with five autophagic adapters genetically deleted
682 (5KO) were treated with 10 μ M ZnPP for the indicated times. Lysates were used for IB analyses.
683 **D.** CMIF analyses. p62WT and p62KO MEF cells were treated with 10 μ M ZnPP or vehicle
684 control for 2 h, and then fixed and stained with anti-I κ B α (green), anti-p62 (magenta) and DAPI
685 (Blue). Insets depict enlarged regions of I κ B α and p62 colocalization.

686

687 **FIGURE 3. ZnPP-elicited I κ B α -loss is due to its sequestration into insoluble cellular**

688 **aggregates. A.** HEK293T cells were transfected with pCMV4-3HA-I κ B α for 40 h, and then

689 treated with 10 μ M ZnPP for 4 h. Cells were then subjected to sequential extraction. 10 μ g of

690 extracts were used for IB analyses. **B.** The same extracts from (**A**) were immunoblotted using

691 three different antibodies each targeting a different region of the same HA-I κ B α protein: Anti-

692 HA-tag, rabbit monoclonal antibody targeting I κ B α N-terminus (N), and rabbit monoclonal

693 antibody targeting I κ B α C-terminus (C). **C.** HEK293T cells were transfected and treated as in **A.**

694 and then subjected to sequential extraction with the following buffers: Cell Signaling lysis buffer

695 (Triton), Cell Signaling lysis buffer supplemented with 1.5 M KCl (HSB). The pellet obtained after

696 HSB-extract was either solubilized with heating in a Laemmli buffer with 4% SDS (SDS) or in

697 urea buffer. 10 μ g of extracts were used for IB analysis.

698

699 **FIGURE 4. IAP-MS of I κ B α -interactome and ZnPP-induced aggregate proteome. A.** Flow-

700 chart of the strategy used to identify a high-confidence I κ B α -interactome. Cells expressing GFP

701 (mEmerald) alone were used as the background control. **B.** Representative Coomassie Blue

702 staining lysates before and after IAP. **C.** 370 high-confidence I κ B α -interactors were plotted with
703 the mean log of enrichment factor against GFP-control on the Y-axis and the *p*-value on the X-
704 axis. Previously known I κ B α -interactors are labeled in red. **D.** Flow-chart of the strategy
705 employed to identify ZnPP-induced aggregate proteome of both HepG2 and HEK293T cells. **E.**
706 Coomassie Blue staining of proteins from sequential Triton, RIPA and urea fractions. HMM
707 fractions of Triton and RIPA extracts and the entire urea fraction (demarcated by the red boxes)
708 were excised from the gel for in-gel digestion and MS analyses (LC-MS/MS). **F.** Venn diagram
709 of proteins enriched at least 2-fold in ZnPP-induced aggregates relative to corresponding
710 controls from HEK293T (HEK) and HepG2 cells indicated 192 proteins as common hits.

711

712 **FIGURE 5. STRING network analyses of proteins common to ZnPP-induced cellular**
713 **aggregates and I κ B α -interactome.** **A.** Venn diagram of I κ B α -interacting proteins identified
714 through LC-MS/MS proteomic analyses of I κ B α -immunoprecipitates upon IAP and/or ZnPP-
715 induced cellular aggregates from HEK293T and HepG2 cells (*as schematized in Fig. 4*). The
716 complete interaction network of 192 common ZnPP-induced protein aggregates was obtained
717 via STRING analyses with the highest confidence score (≥ 0.9). Network statistics are
718 summarized in the inset. Functional enrichments are annotated with color-lined boxes with the
719 false discovery rates (FDR) included. Of these, the 47 I κ B α -interacting proteins are highlighted
720 in yellow. **B.** The corresponding heat map percentile ranked according to the individual fold-
721 enrichment of these 47 I κ B α -interacting proteins common to ZnPP-induced aggregates in
722 different experiments. C1-I κ B α IP represents mean fold-enrichment from C1-mEmerald-I κ B α
723 IAP against C1-Emerald (GFP) background control ($n = 3$). The other sets represent fold-
724 enrichment of proteins in cellular aggregates at 2 h and 24 h post ZnPP-treatment of HepG2
725 and HEK293T cells relative to corresponding controls. I κ B α BAR in +ZnPP/-ZnPP pellet

726 aggregates represents fold-enrichment of $\text{I}\kappa\text{B}\alpha$ -antibody mediated IP of biotinylated proteins in
727 cellular aggregates at 2 h after ZnPP-treatment of HEK293T cells relative to vehicle controls.
728 Proteins previously found in aggregates from other disease models and/or human pathological
729 samples are indicated in red. * Proteins found in liver aggregates from mouse and zebra fish
730 protoporphyric models [13, 36, 37]. # Proteins previously found in protein aggregates of
731 pathological samples from human MS and/or Lewy bodies of Parkinson's disease [53, 55]. &
732 Proteins previously found in aggregates/ or mislocalized in ALS/FTLD patient samples [54].

733

734 **Figure 6: Nup153 is an $\text{I}\kappa\text{B}\alpha$ -interacting protein that is a major target of ZnPP-elicited**
735 **aggregation.** **A.** HEK293T cells and HepG2 cells were treated with 10 μM ZnPP for 2 h. Cells
736 were sequentially extracted with Triton and urea buffers. 10 μg of extracts were used for
737 Nup153 and $\text{I}\kappa\text{B}\alpha$ IB analyses, with actin as the loading control. **B.** Co-immunoprecipitation (Co-
738 IP) of overexpressed $\text{I}\kappa\text{B}\alpha$ with endogenous Nup153. HEK293T cells were transfected with C1-
739 GFP control vector, or C1-GFP- $\text{I}\kappa\text{B}\alpha$ vector, or a mock control for 40 h. Co-IP of cytosolic
740 fractions (CER) and nuclear fractions (NER) with GFP-trap followed by Nup153 and $\text{I}\kappa\text{B}\alpha$ IB
741 analyses, with actin as the loading control, and GAPDH and HistoneH3 (H3) as fractionation
742 controls. **C.** Co-IP of endogenous $\text{I}\kappa\text{B}\alpha$ with endogenous Nup153. HepG2 cells were treated
743 with 20 ng/ml $\text{TNF}\alpha$ for the indicated times followed by co-IP of whole cell lysates with $\text{I}\kappa\text{B}\alpha$
744 antibody or control IgG and IB of Nup153 and $\text{I}\kappa\text{B}\alpha$ with actin as the loading control. **D.** Mouse
745 hepatocytes were either untreated or pretreated with 20 ng/ml $\text{TNF}\alpha$ for 1 h and then treated
746 with 10 μM ZnPP or left untreated for the indicated times. Cell lysates were used for IB analyses
747 of Nup153 and $\text{I}\kappa\text{B}\alpha$ with actin as the loading control. $\text{I}\kappa\text{B}\alpha$ contents relative to 0 h controls were
748 quantified (Mean \pm SD, n = 3, ** P<0.01, * P<0.05). **E.** CMIF analyses. HepG2 cells were treated
749 with vehicle control (Ctrl), or 20 ng/ml $\text{TNF}\alpha$ for 0.5 h or 1 h. Some $\text{TNF}\alpha$ -treated cells were also

750 treated with 10 μ M ZnPP 20 min after TNF α -addition and incubated for another 40 min (TNF α +
751 ZnPP 1h). Cells were fixed and stained with anti-p65/anti-rabbit-Alexa-488 IgGs (green) and
752 anti-I κ B α /anti-mouse Alexa-647-conjugated IgGs (magenta) and DAPI. Images were obtained
753 under 100X lens. The same slides were then observed under wide-field microscope using 60X
754 lens to quantify the percentage of cells with predominant nuclear p65 accumulation. Cells (>600)
755 were assessed at each experimental condition (Mean \pm SD, n = 3).

756

757 **Fig. 7. Effects of siRNA knockdown of Nup153 (A) and RanBP2 (B) on TNF α -elicited I κ B α**

758 **nuclear import.** HEK293T cells were transfected with control siRNA (Ctrl) or NUP153 siRNA (A)

759 or RanBP2 siRNA (B) or for 48 h, and then treated with 20 ng/ml TNF α for the indicated times.

760 Cytosol and nuclear extracts were used for IB analyses. I κ B α content was plotted over time. C.

761 HEK293T cells were transfected with control siRNA (Ctrl) or NUP153 siRNA for 48 h, and then

762 treated with 10 μ M ZnPP for the indicated times. Cell lysates were used for IB analyses. D.

763 HEK293T cells were transfected with control siRNA (Ctrl) or RanBP2 siRNA for 48 h, and then

764 treated with 10 μ M ZnPP for the indicated times. Cell lysates were used for IB analyses.

765

766 **Fig. 8. Effects of I κ B α siRNA knockdown on I κ B β -levels and constitutive (A) and**

767 **ZnPP-induced NF κ B-activation (B).** siRNA knockdown and EMSA analyses were conducted

768 as detailed in Supplementary Methods. The marked hepatic I κ B β -upregulation coupled with the

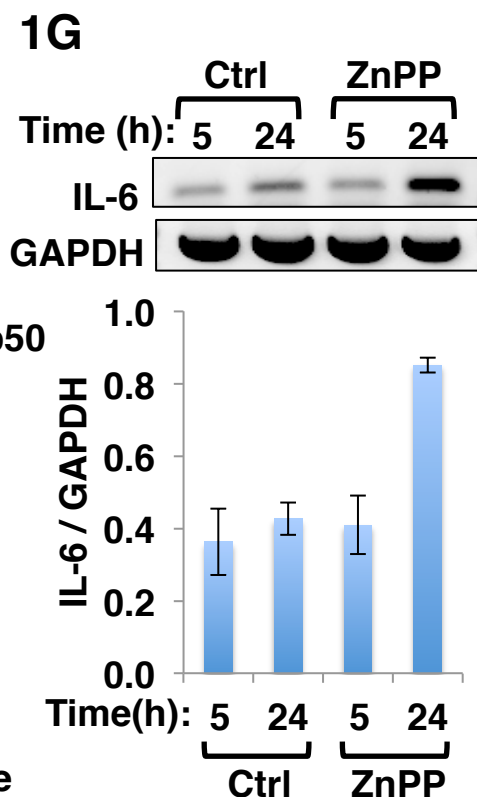
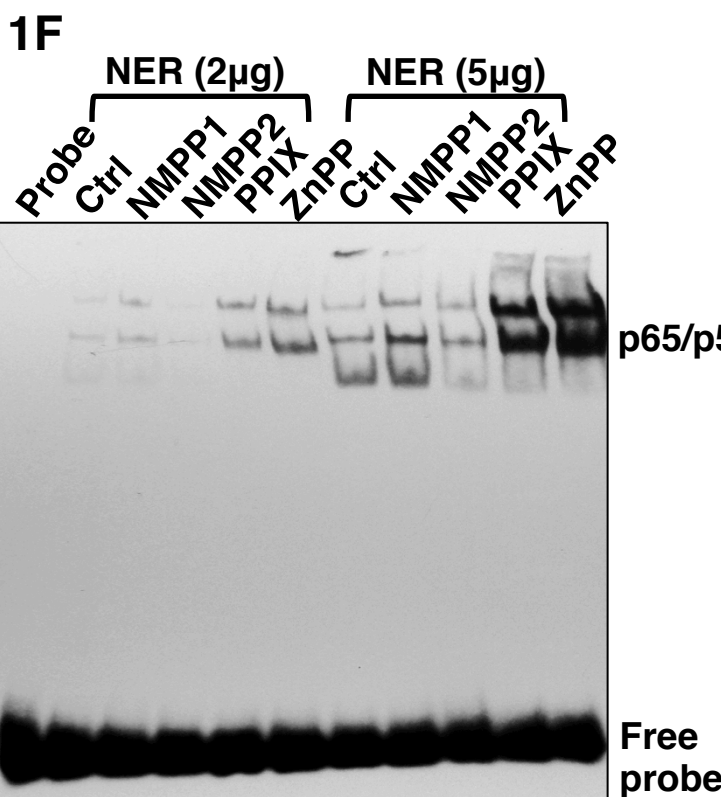
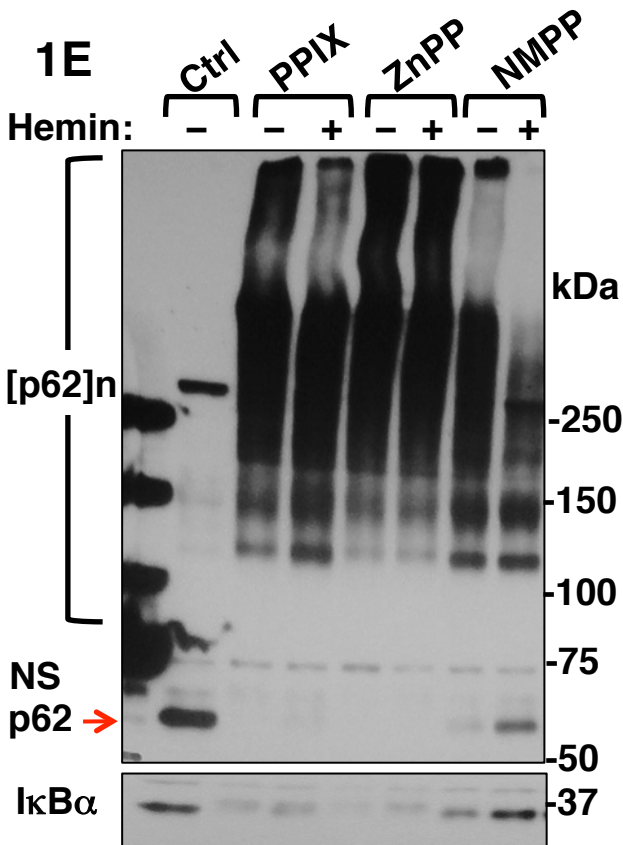
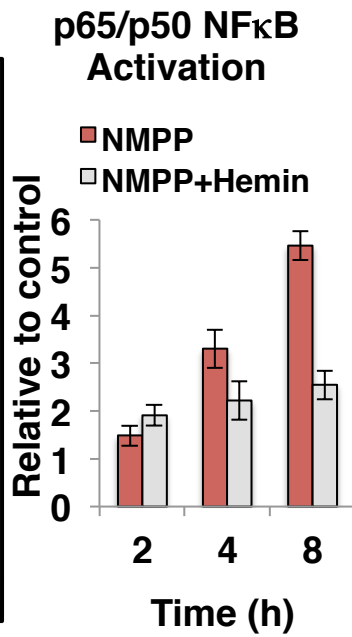
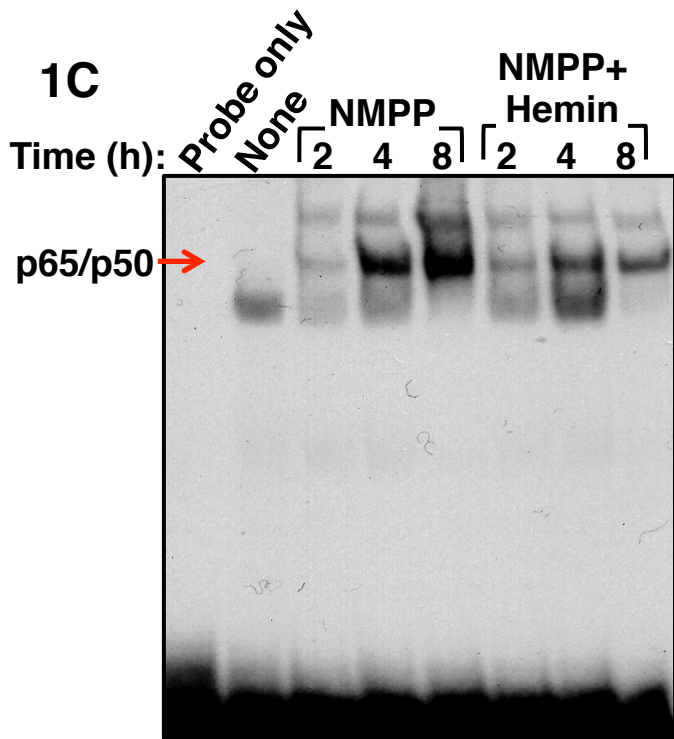
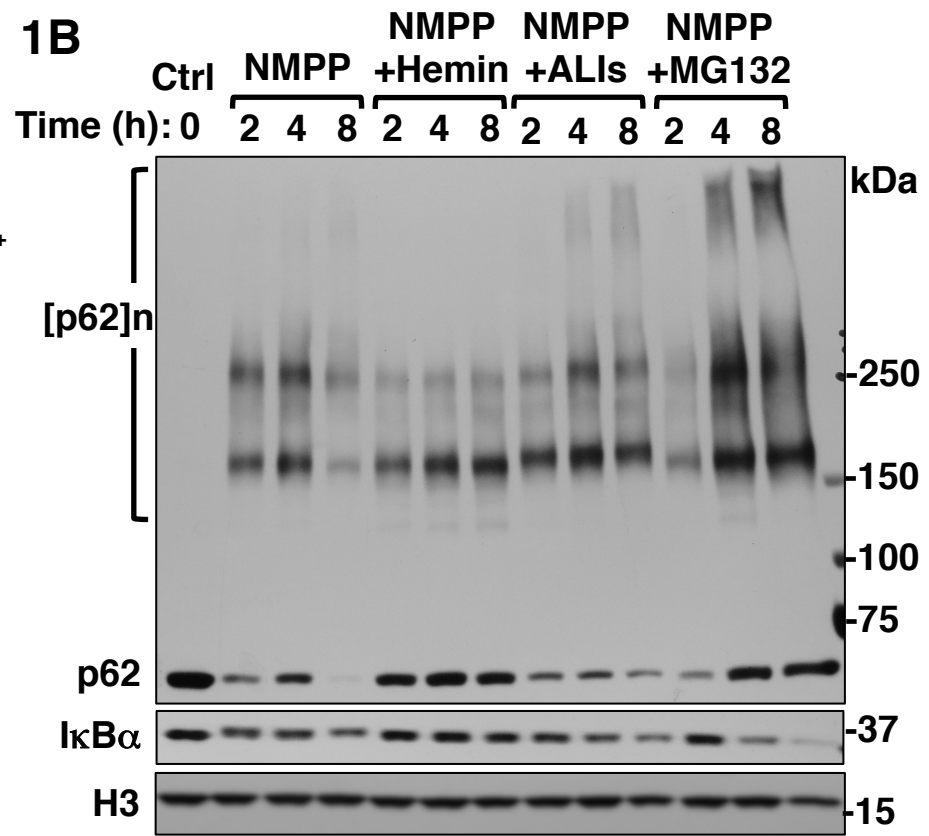
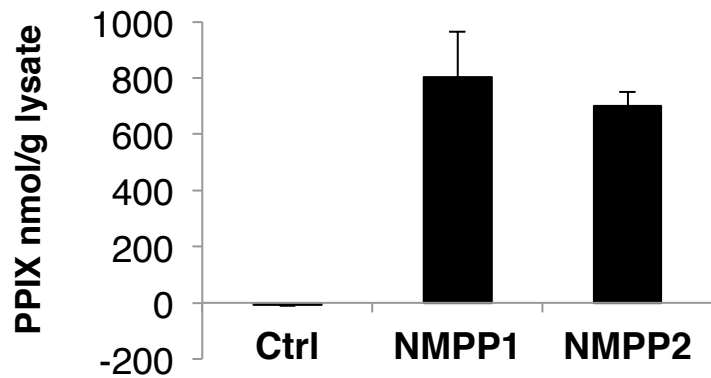
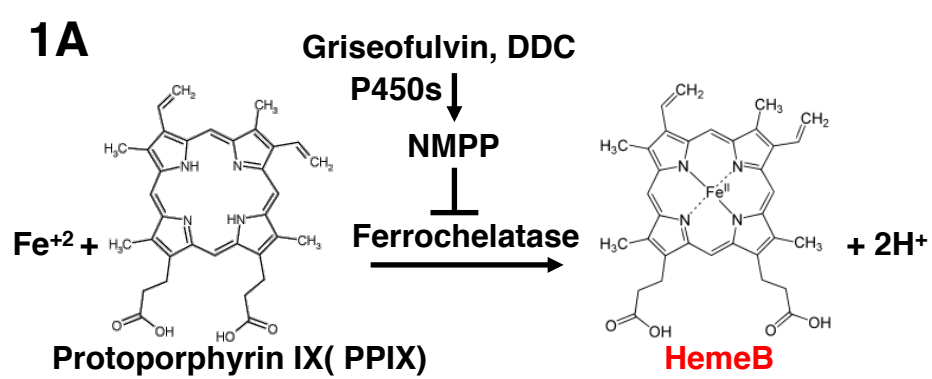
769 relatively less pronounced NF κ B-activation observed upon I κ B α -siRNA knockdown versus

770 ZnPP-treatment led to the examination of whether I κ B β was similarly sequestered by ZnPP as

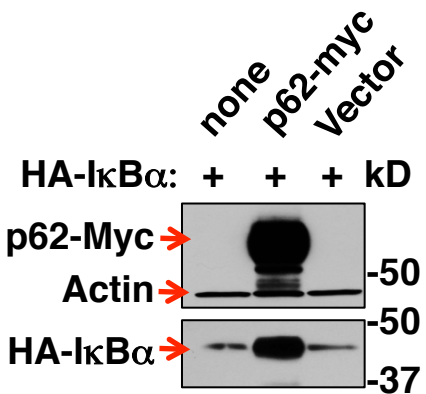
771 I κ B α (C). Proteolytic inhibitors used as in Fig. 2D. (D). qRT-PCR analyses of mRNA from intact

772 livers of mice injected i.p., daily with ZnPP (50 μ mol/kg) or vehicle controls (Ctrl) for 7 d (Mean,

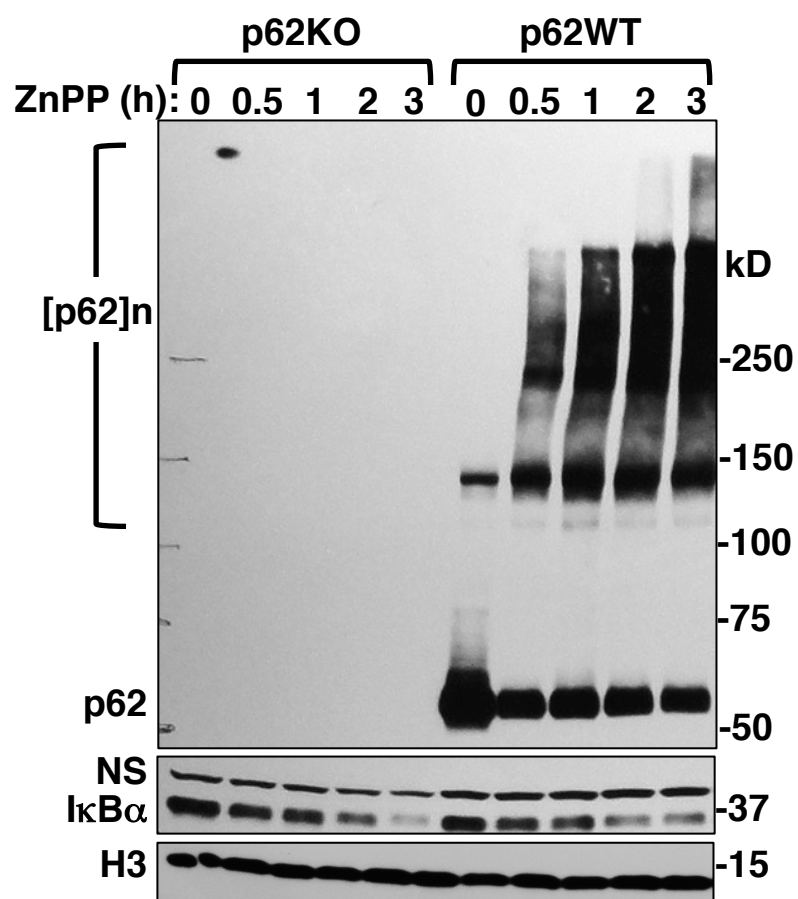
773 n = 2). SPP1, osteopontin or secreted phosphoprotein 1.



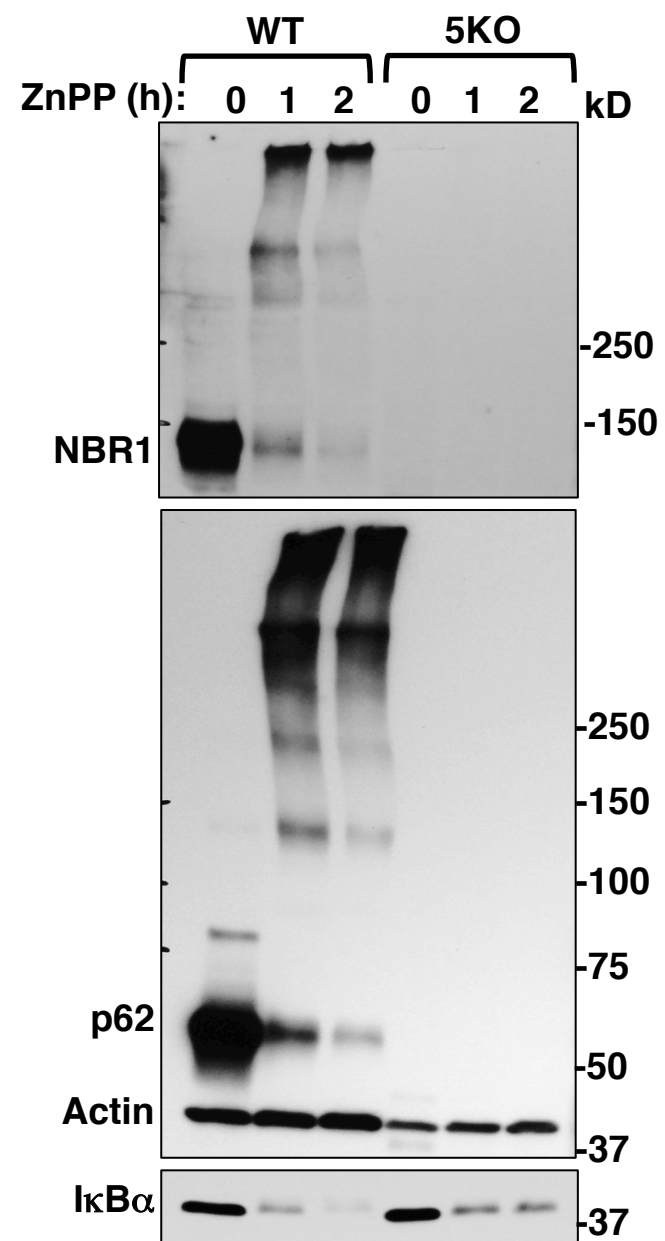
2A



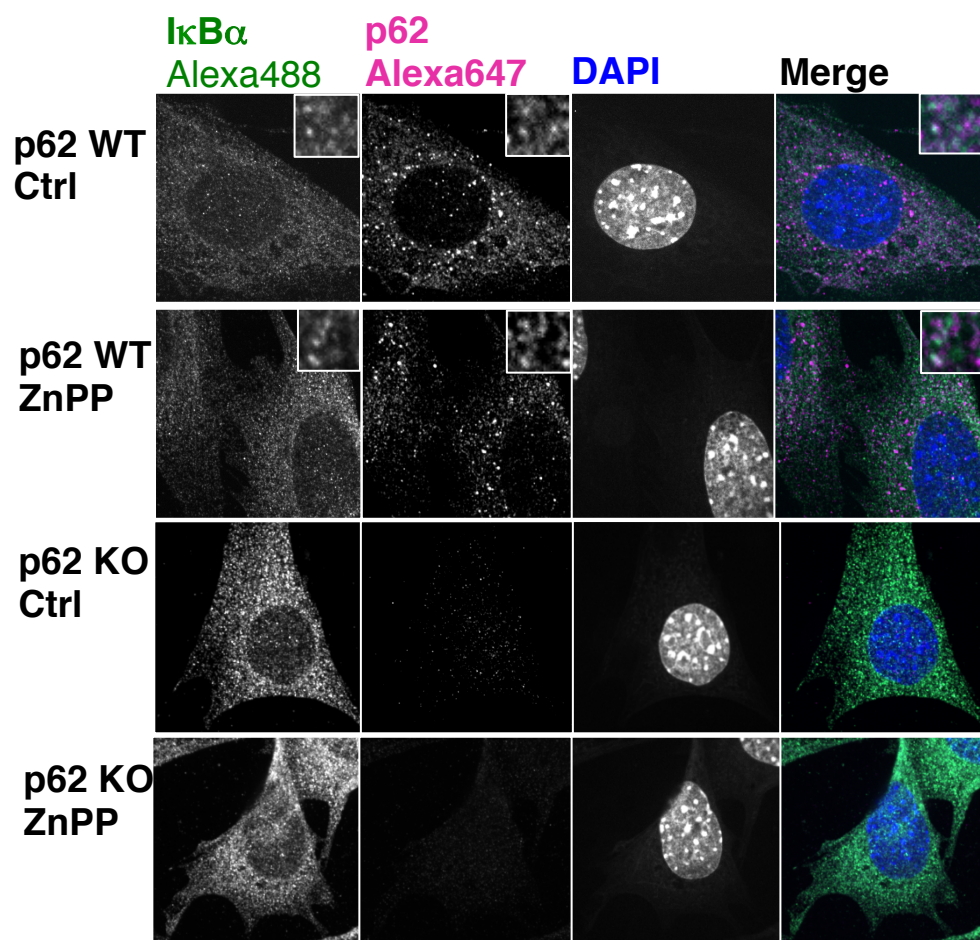
2B

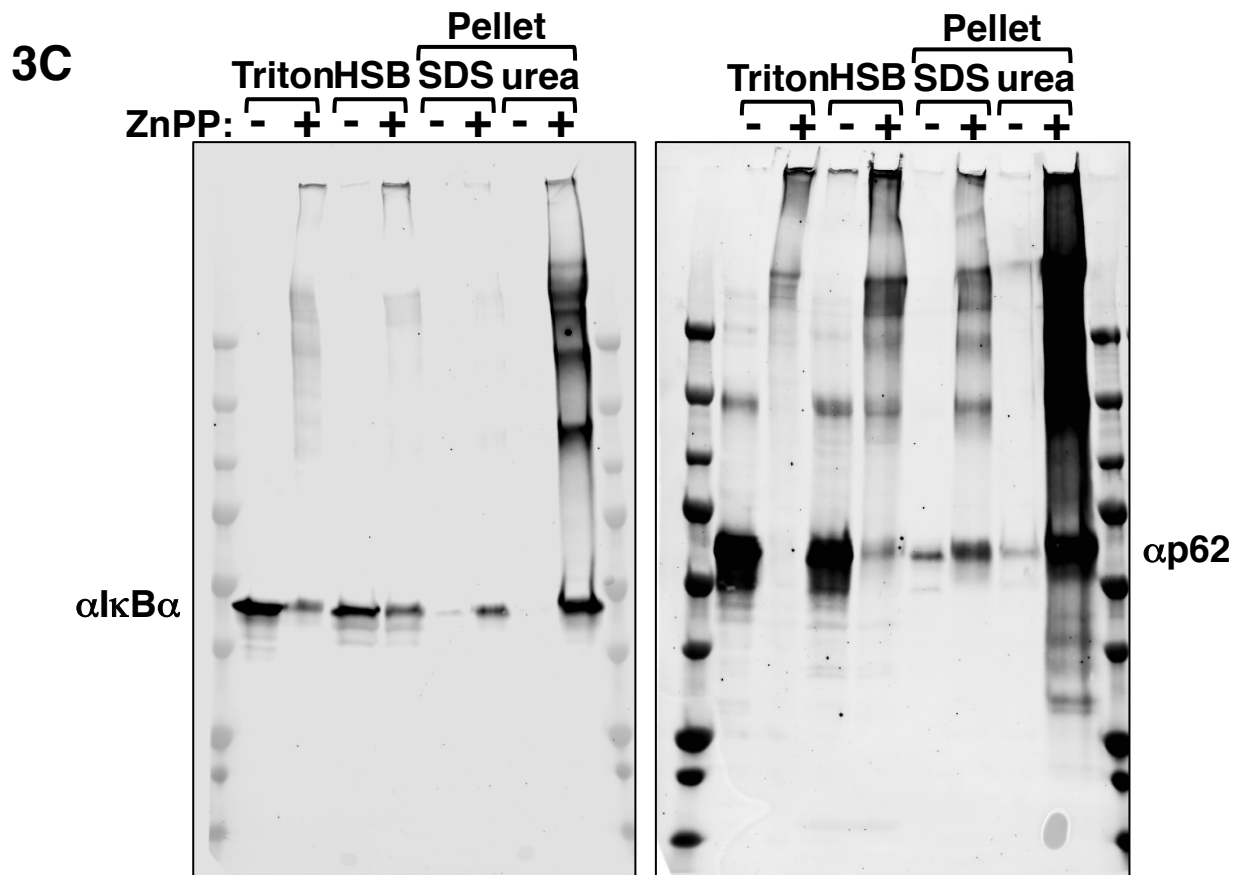
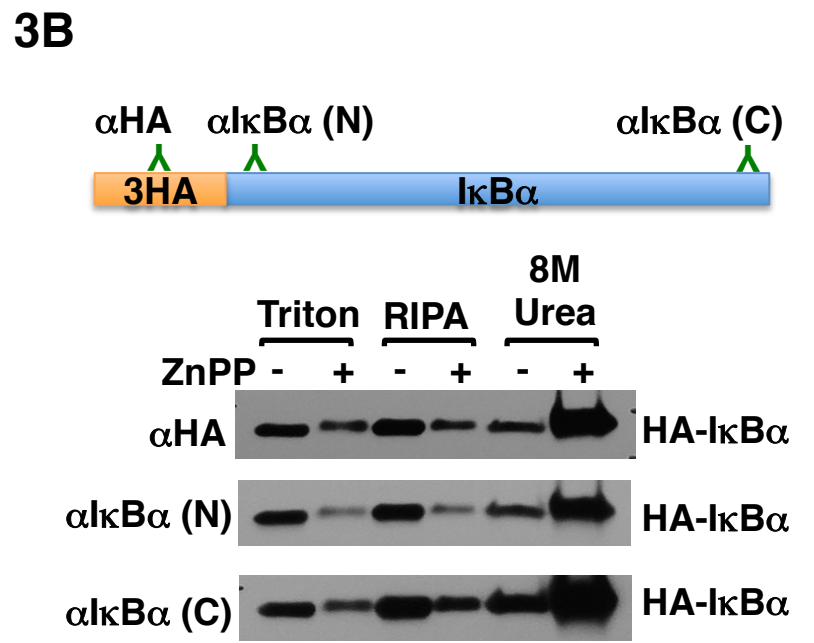
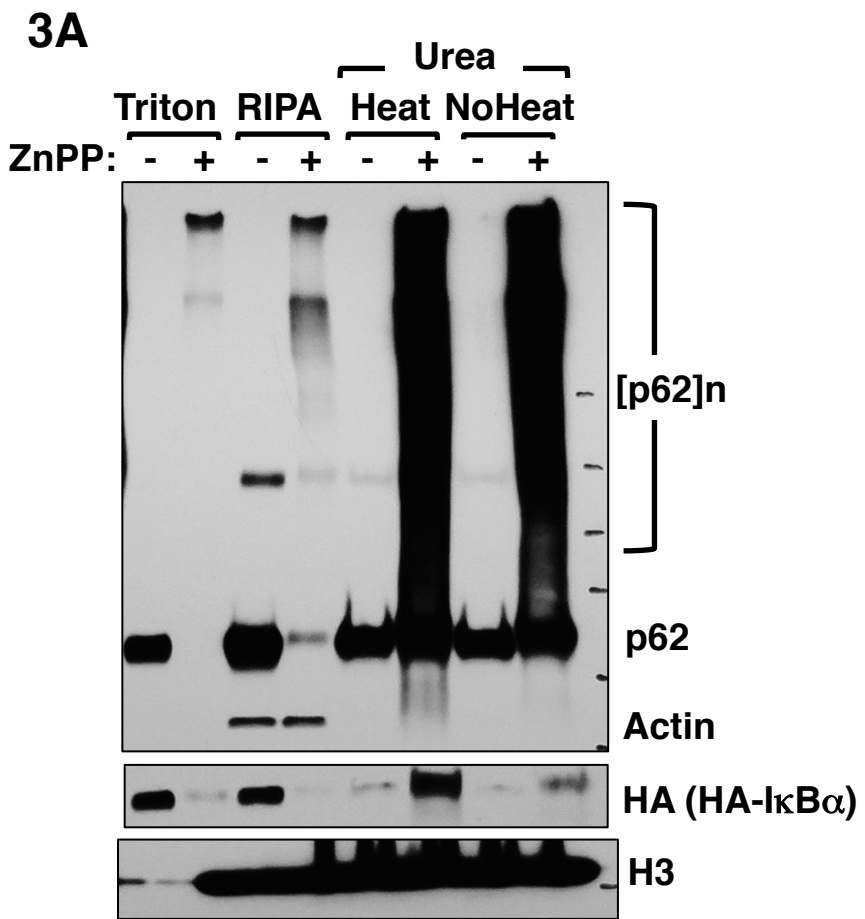


2C

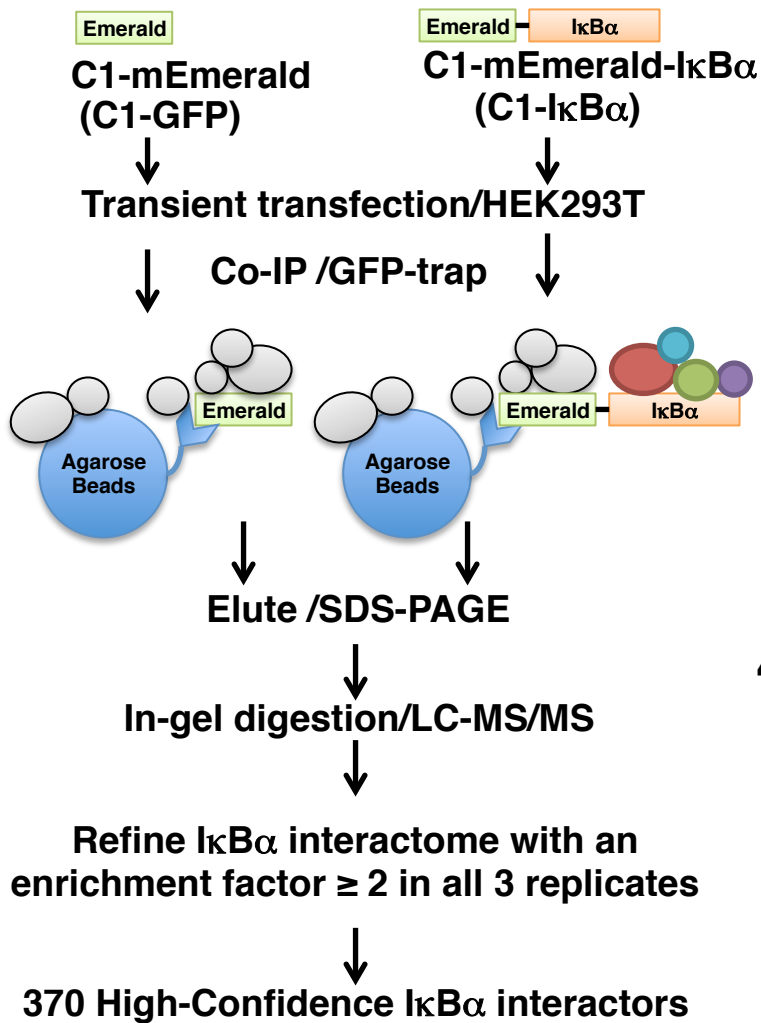


2D

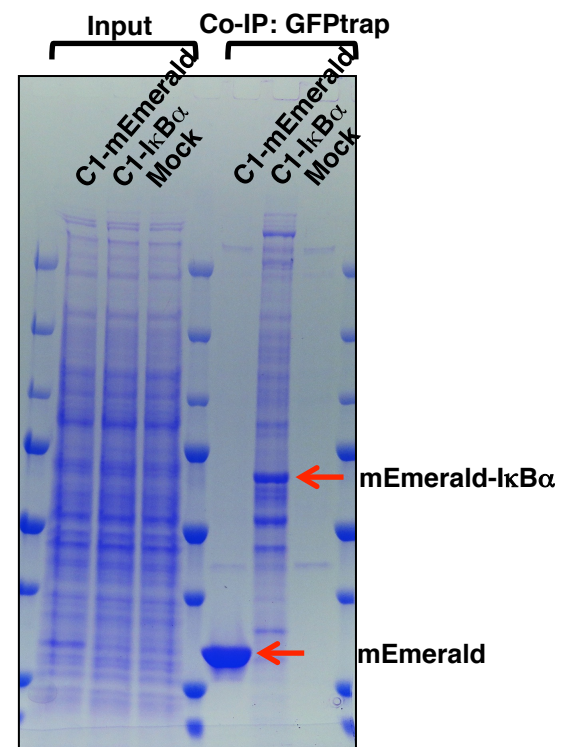




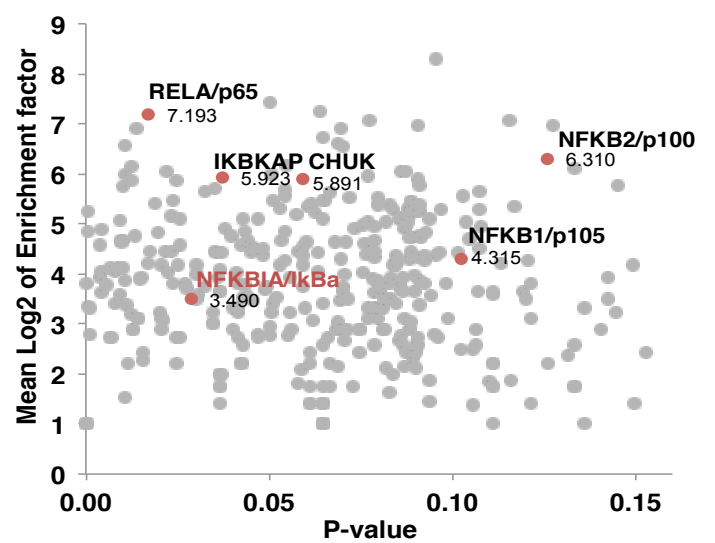
4A



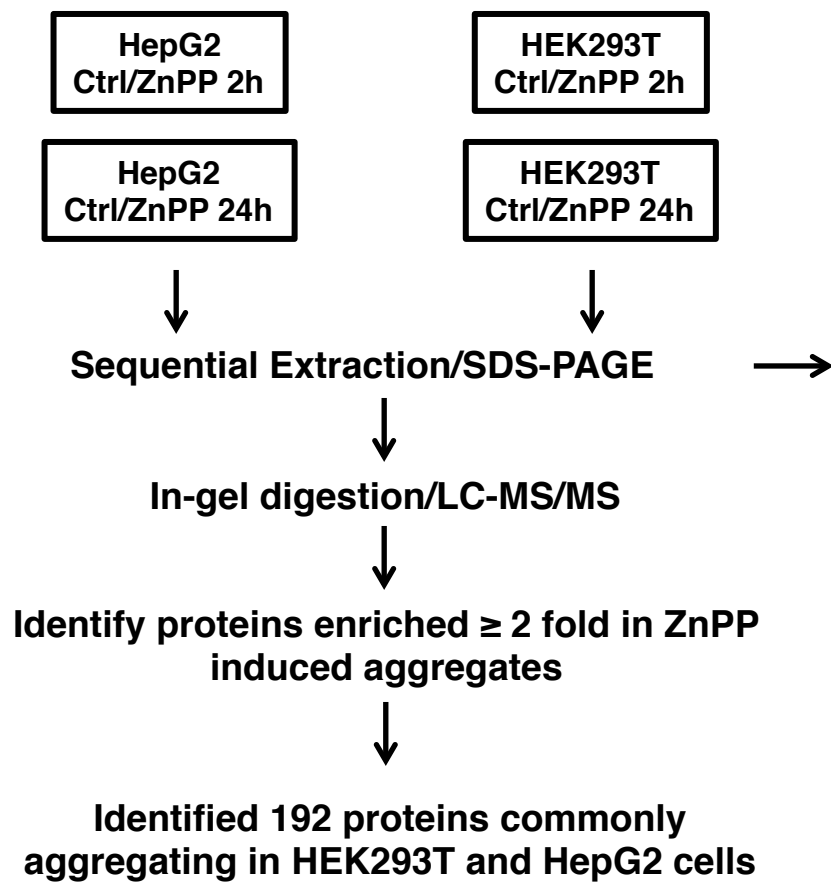
4B



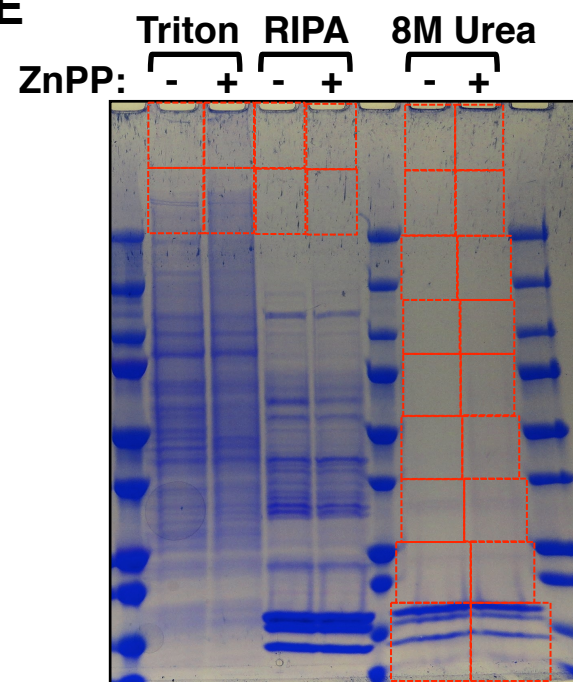
4C



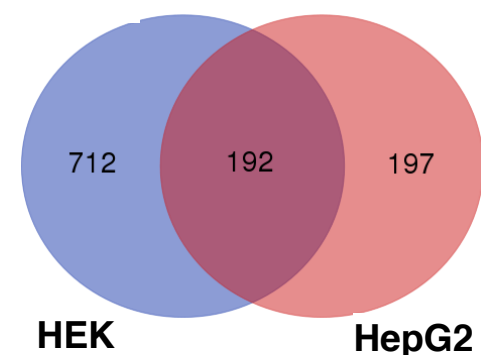
4D



4E



4F



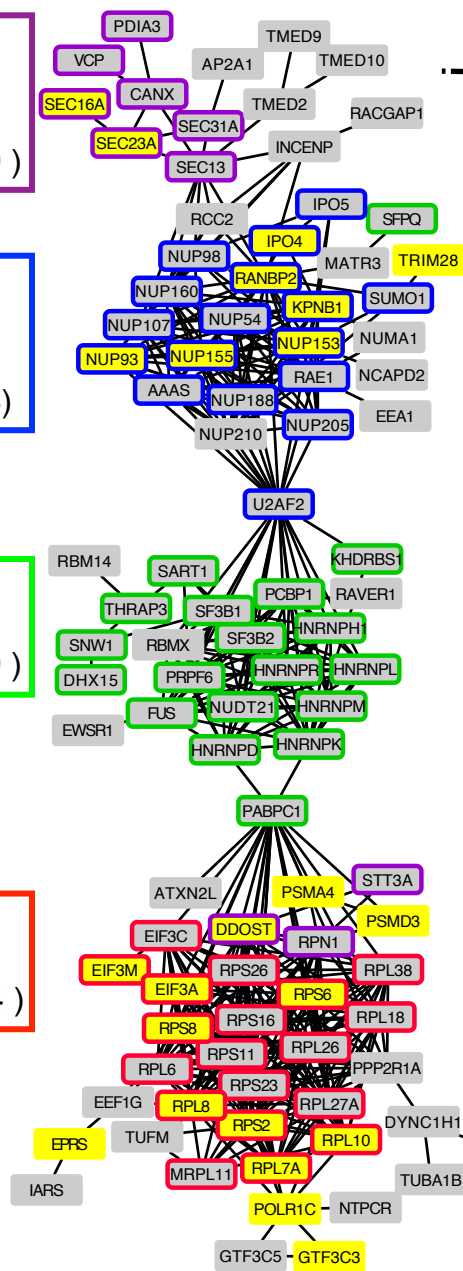
5A

Protein Processing in ER
(FDR 2.78E-09)

Nucleo-cytoplasmic Transport
(FDR 2.64E-08)

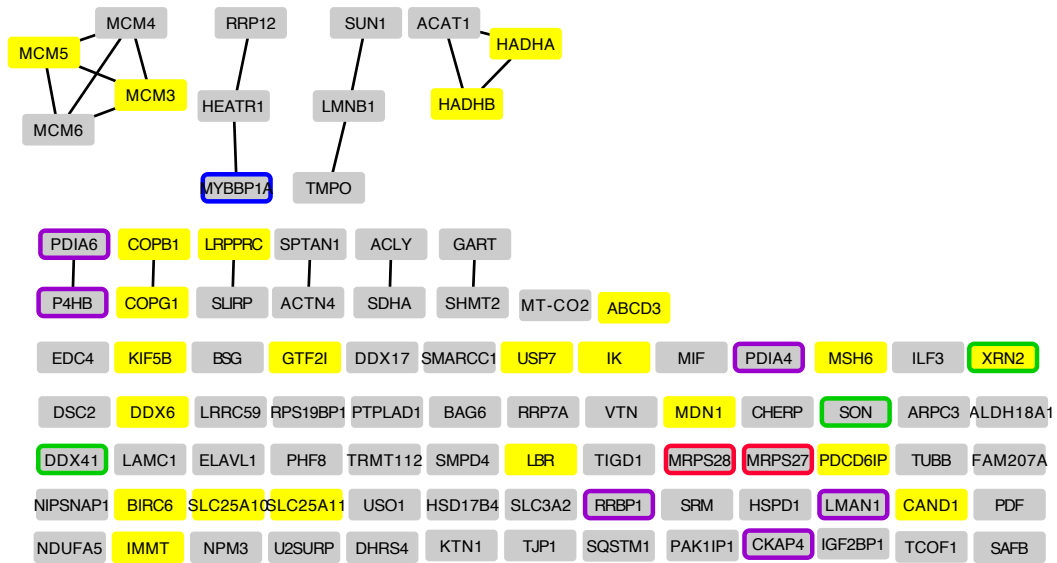
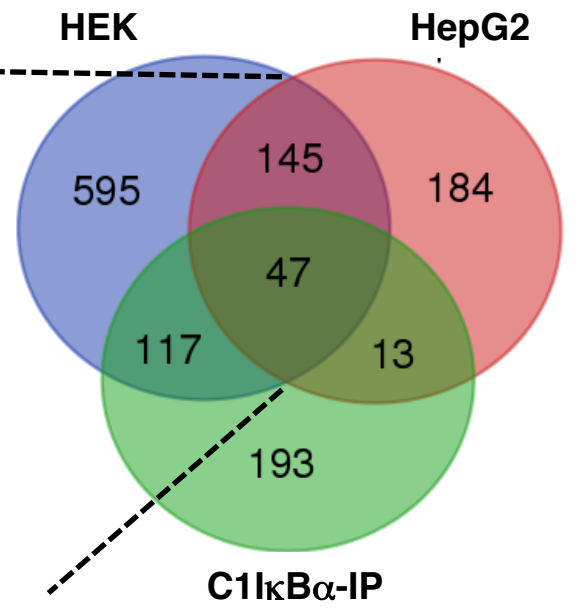
mRNA Processing
(FDR 7.01E-09)

Translational Initiation
(FDR 4.66E-14)

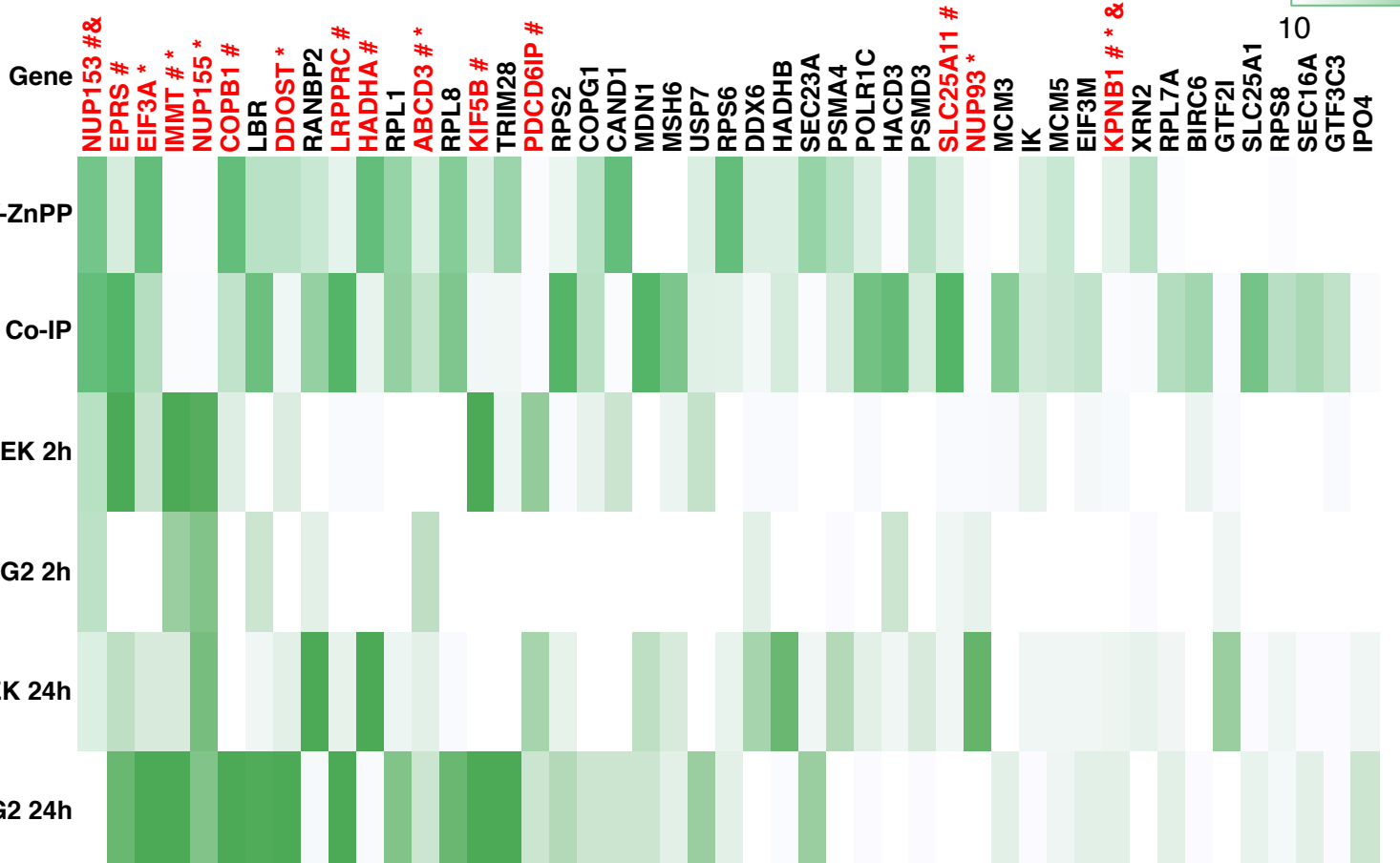
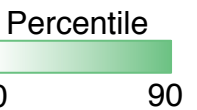


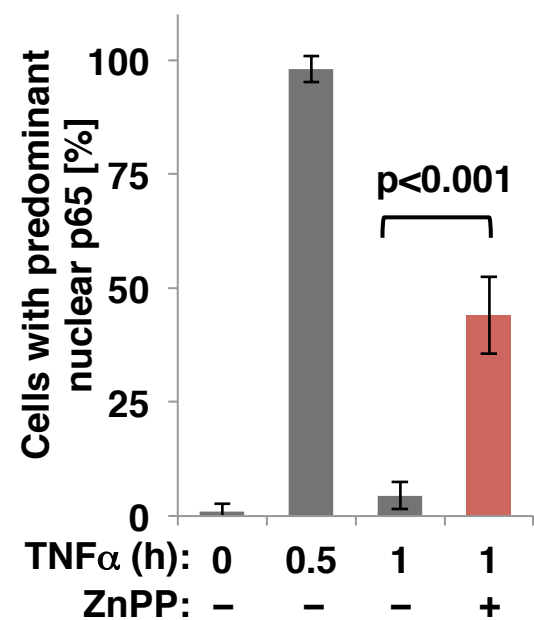
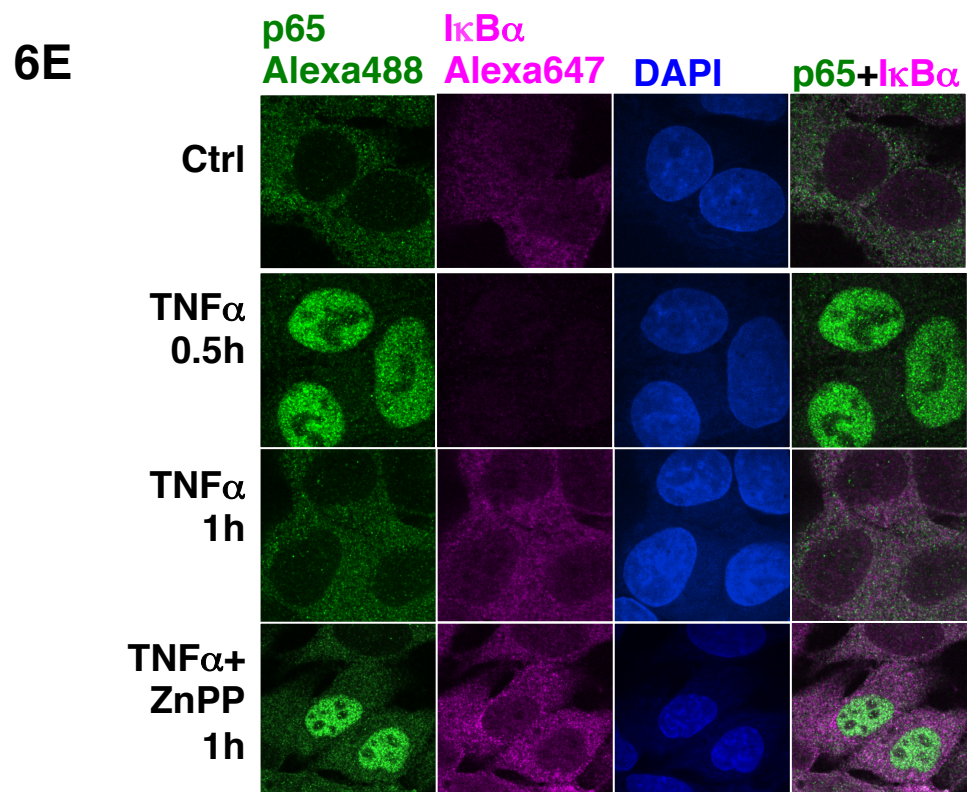
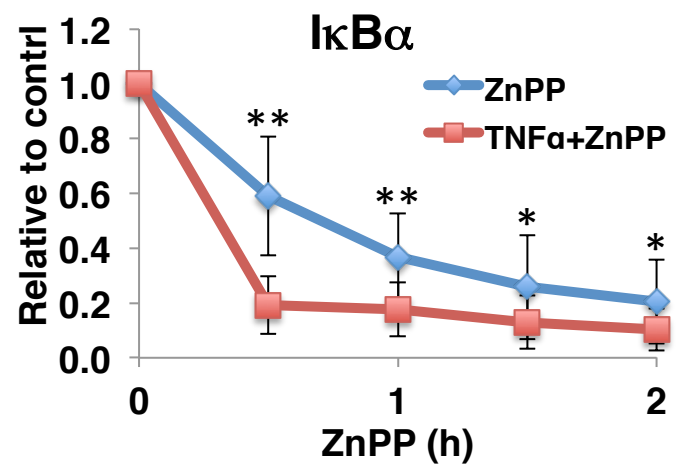
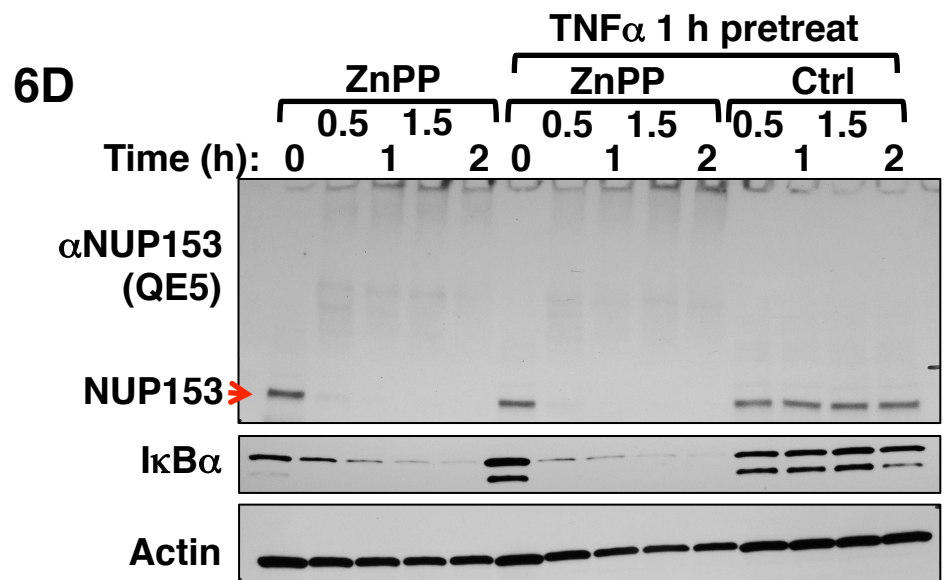
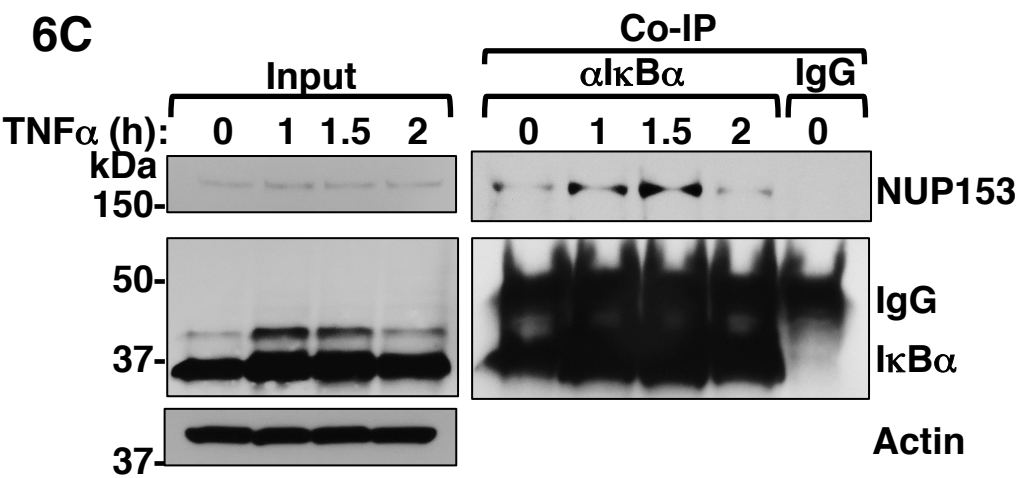
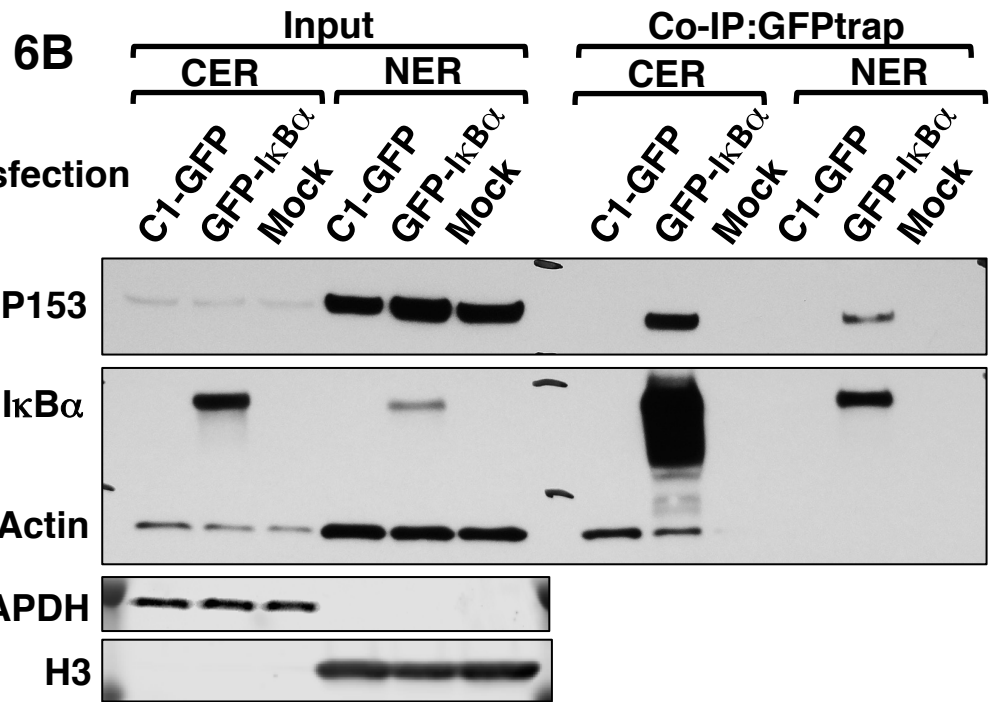
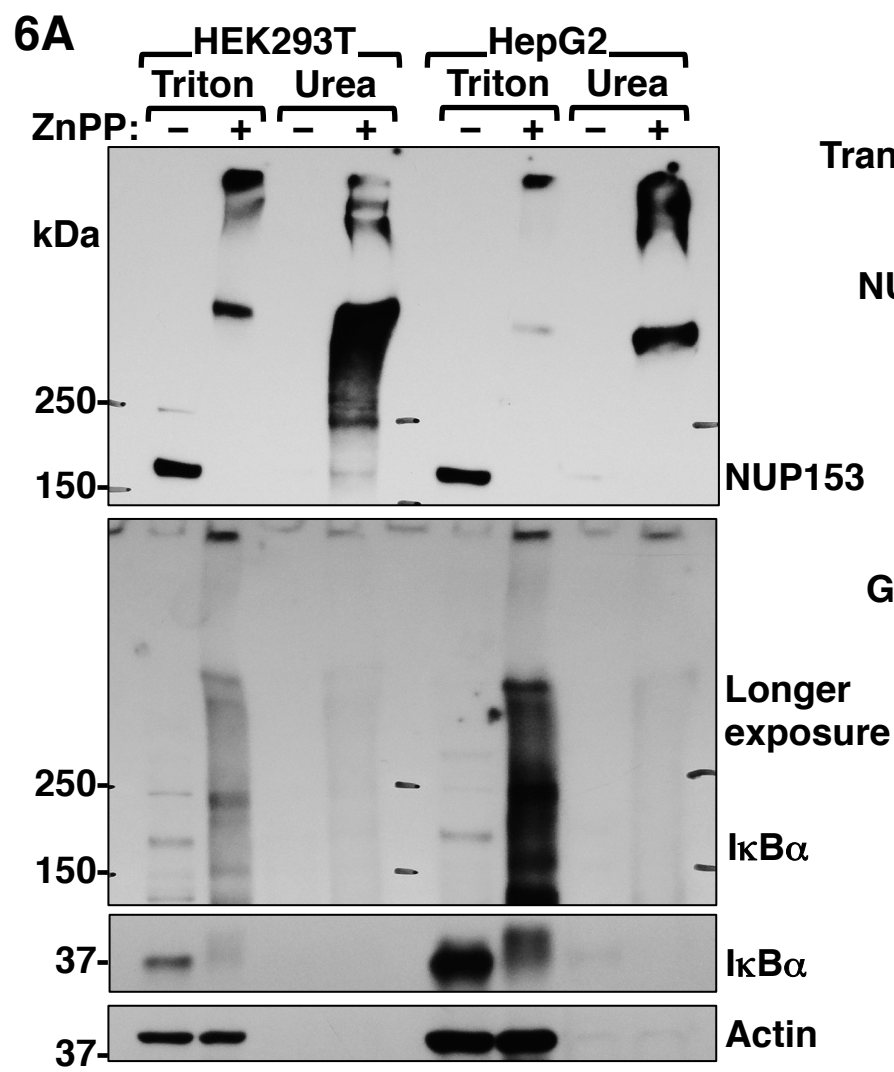
Network Stats

number of nodes:	189
number of edges:	493
average node degree:	5.22
average local clustering coefficient:	0.527
expected no. of edges:	118
PPI enrichment p-value:	<1E-16

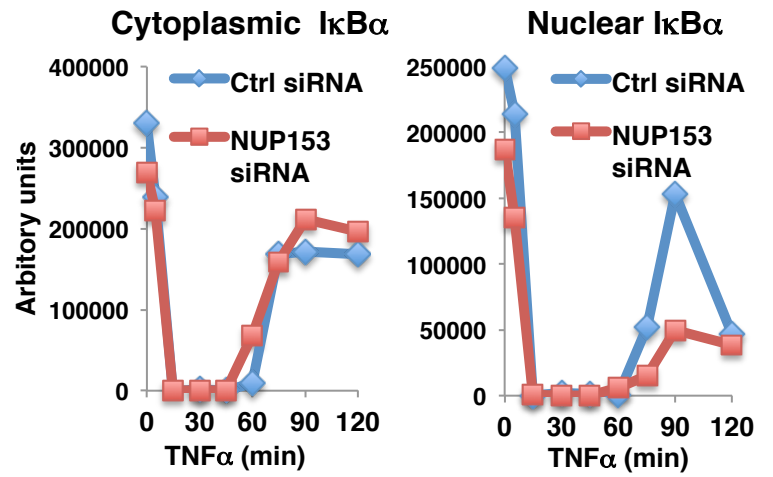
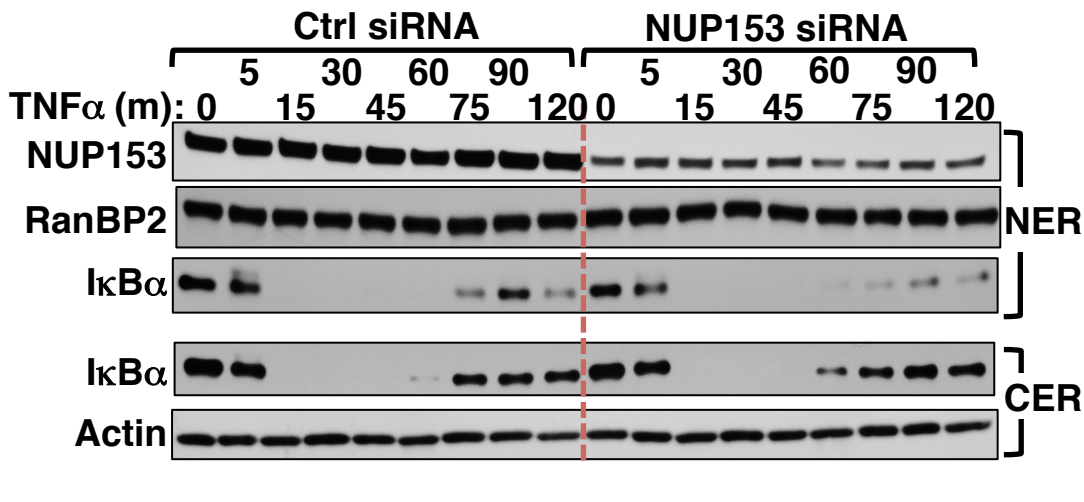


5B

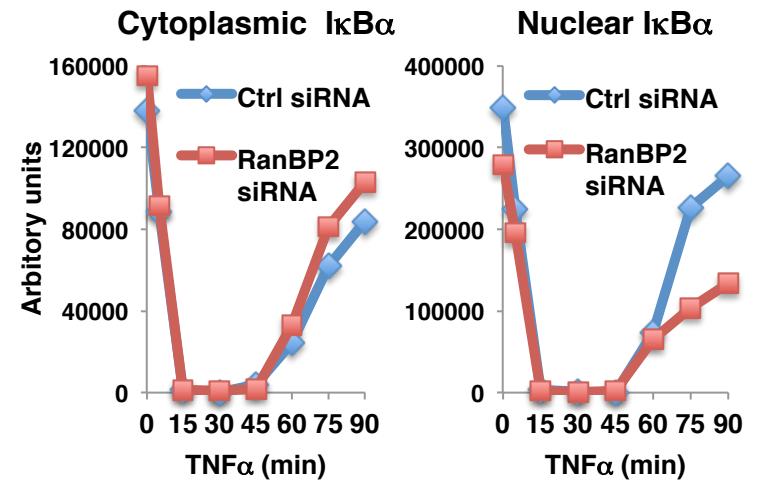
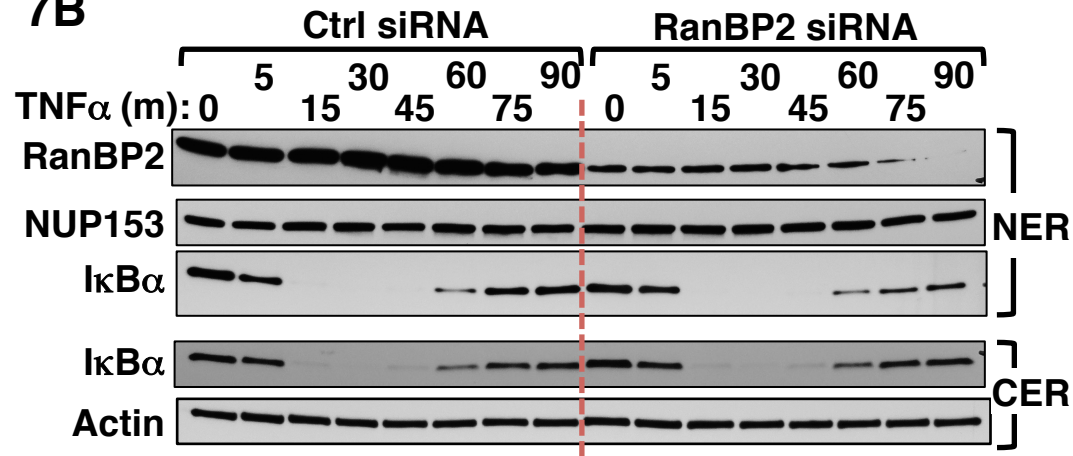




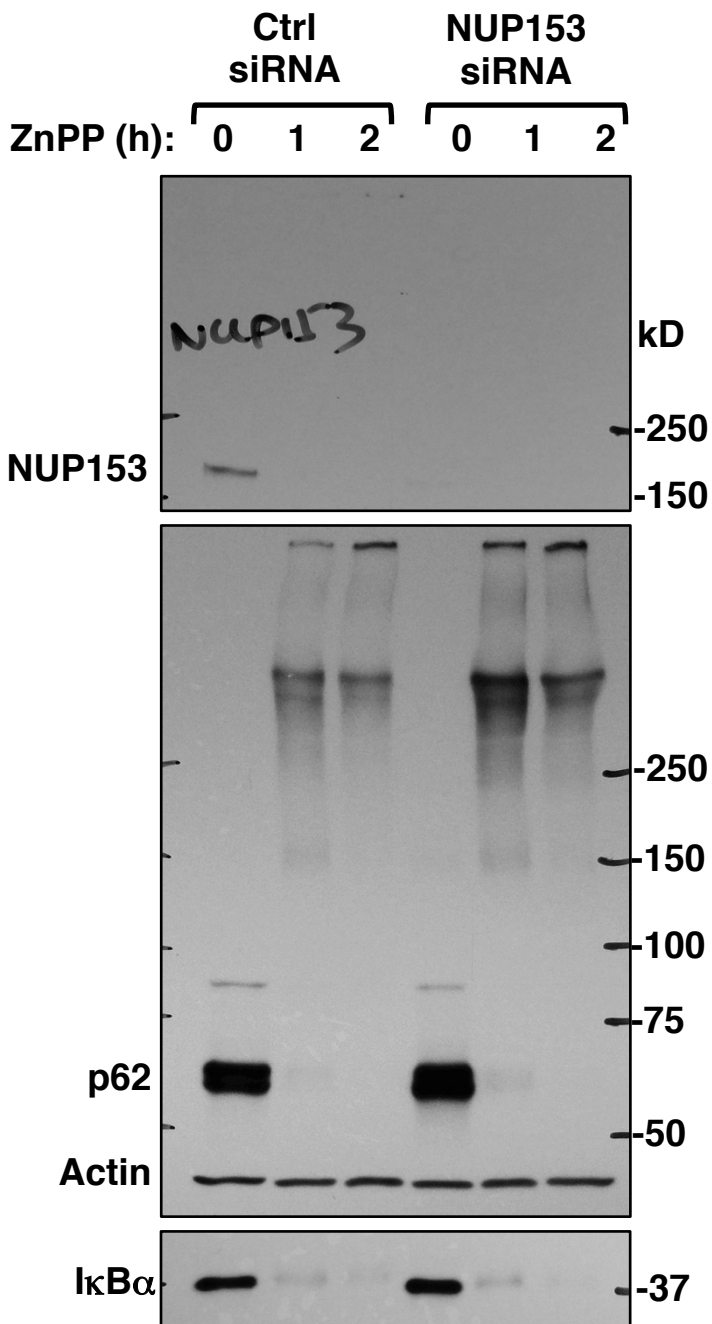
7A



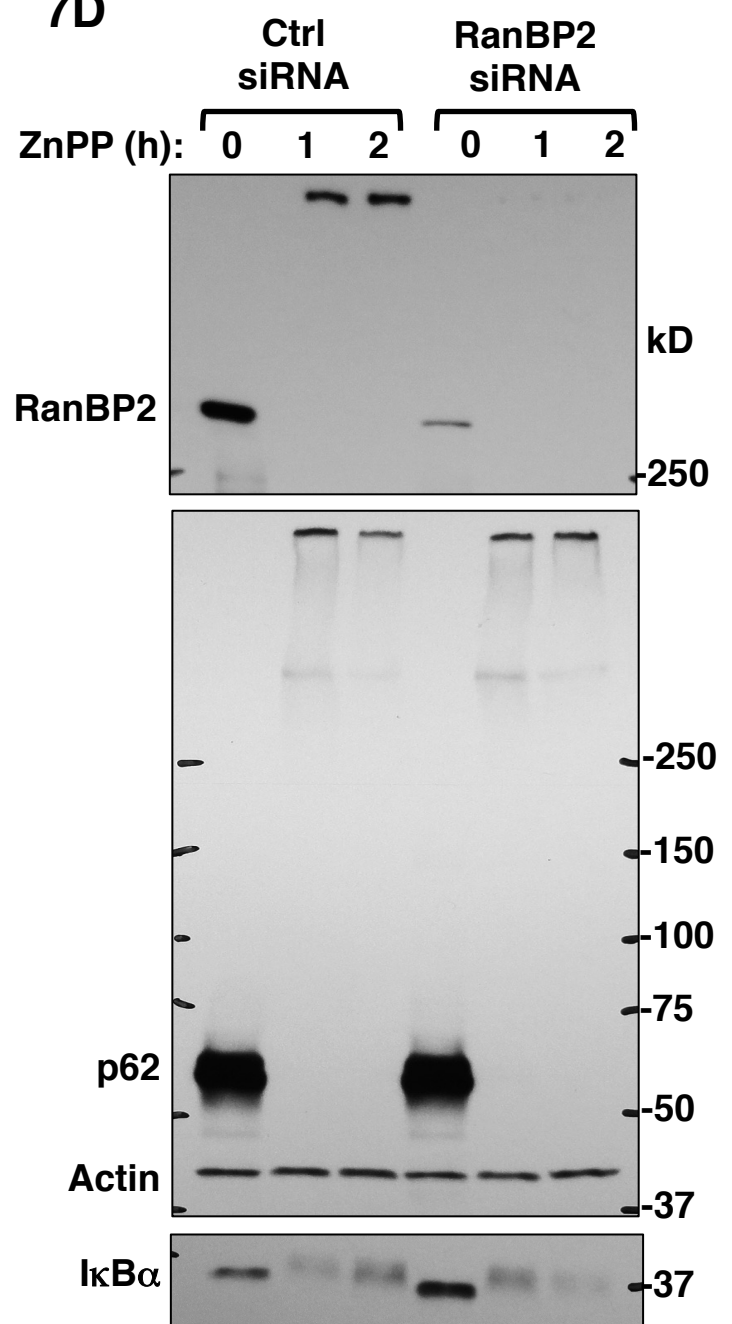
7B

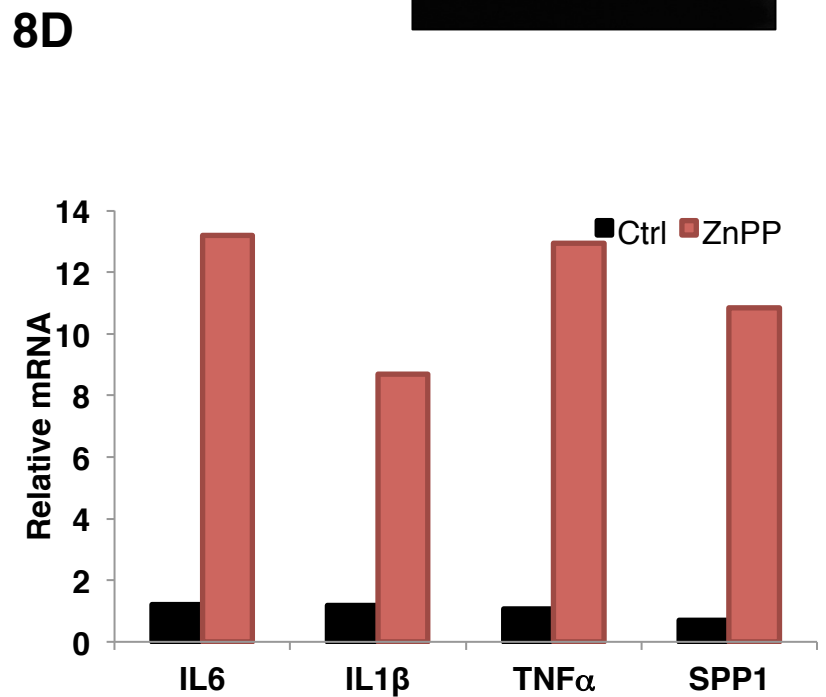
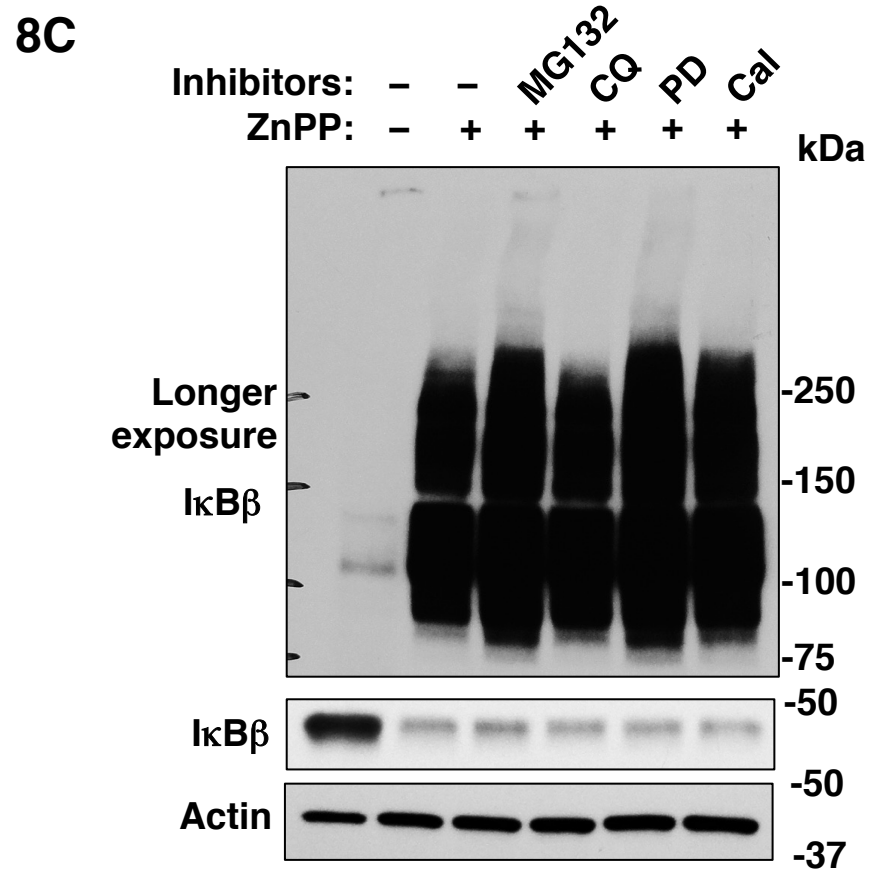
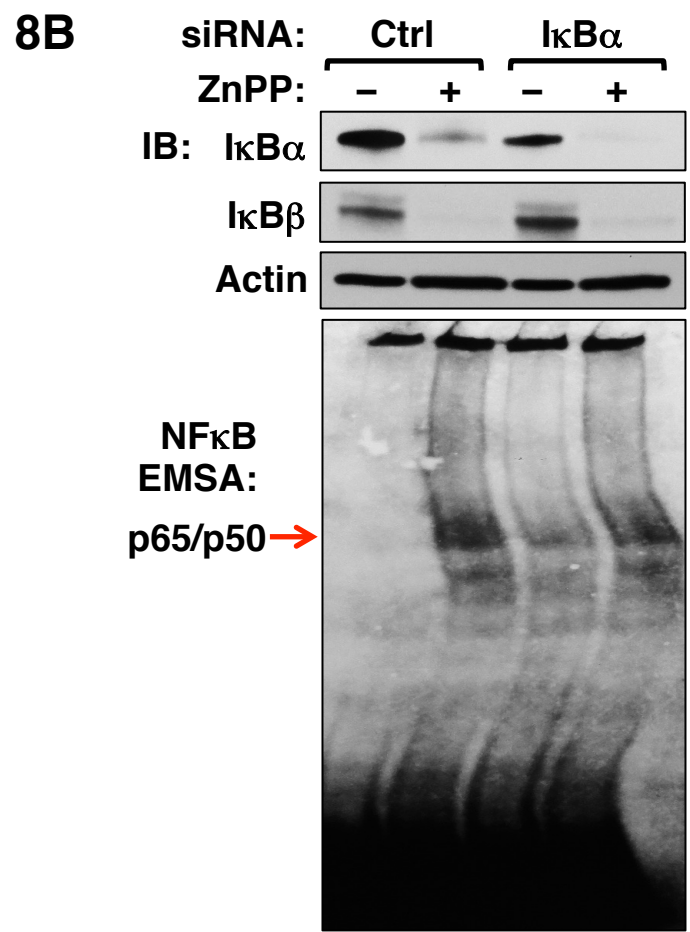
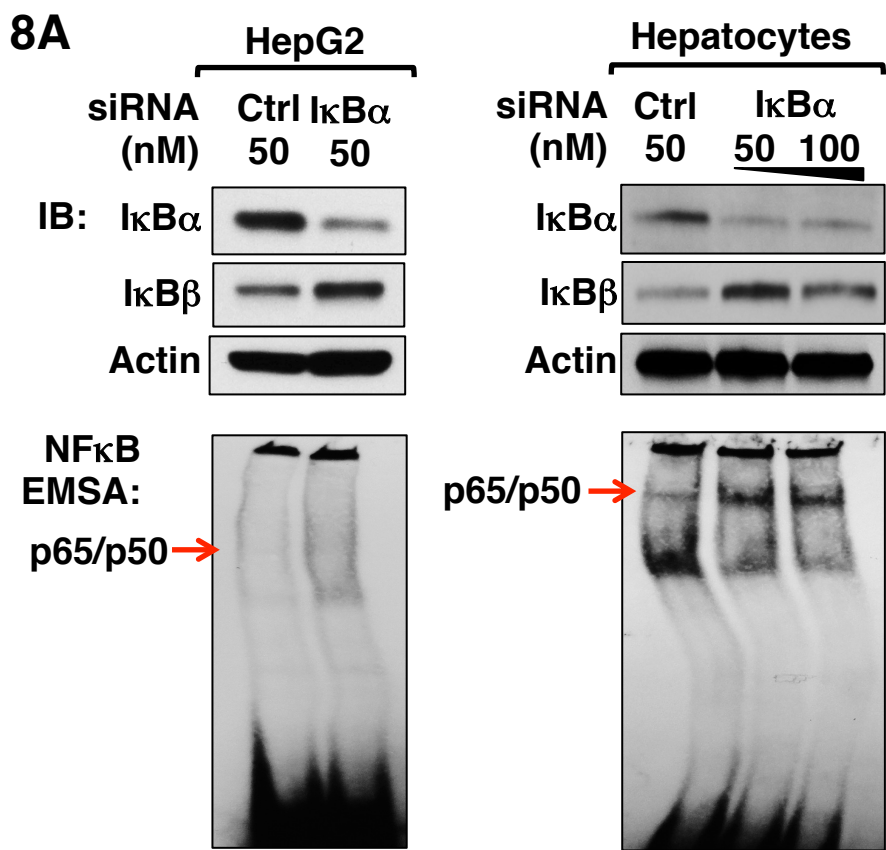


7C



7D





Supplementary Results & Discussion:

Results:

NMPP-elicited I κ B α -loss is independent of HRI eIF2 α -kinase activation: The concurrence of I κ B α loss and NF- κ B activation and its attenuation by hemin-treatment led us to consider whether NMPP-elicited heme depletion was responsible for these findings. Conceivably, heme depletion could activate the hepatic heme-sensor HRI eIF2 α kinase resulting in the translational suppression of I κ B α and consequent NF- κ B-activation. Similar I κ B α translational suppression and consequent NF- κ B-activation has been documented upon specific activation of the other cellular eIF2 α kinases [1, 2]. Indeed, in parallel with I κ B α -loss (Fig S2A), NMPP treatment increased the relative ratio of phosphorylated eIF2 α (eIF2 α P) over basal eIF2 α levels, indicating HRI activation [3]. However, NMPP-treatment of cultured hepatocytes from cultured hepatocytes from HRI WT (HRI^{+/+}) and knockout (KO; HRI^{-/-}) mice elicited a comparable I κ B α , excluding causal HRI activation (Fig. 1D).

ZnPP-elicited I κ B α -loss is independent of autophagy, calpain-mediated proteolysis and reactive oxygen species (ROS): Given the reported I κ B α -degradation via ALD [4] and the known p62-role in this process [5], we conclusively excluded ALD in this process by documenting that knockout of the essential autophagic gene ATG5 failed to mitigate ZnPP-elicited I κ B α loss (Fig. S2B). Because of possible calpain-mediated I κ B α -degradation [6, 7], we also excluded its involvement by documenting that knockout of the calpain-degradation pathway (capn4 KO MEF cells) failed to abrogate ZnPP-elicited I κ B α loss (Fig. S2C). These findings coupled with those with ALD and calpain inhibitors (Fig. 2D) revealed that neither ALD nor calpain degradation played any role in this I κ B α loss. Furthermore, through the use of various ROS-quenchers (Fig. S3), we excluded any possible PPIX-photoactivation and consequent ROS-mediated oxidative stress in this I κ B α -loss [8].

Discussion:

The precise mechanism of the ZnPP-elicited I κ B-protein sequestration is currently unknown, but some plausible mechanisms are presented. The fact that newly synthesized I κ B α is particularly vulnerable to such ZnPP-sequestration implicates the involvement of its intrinsic disordered domains at a stage when it has not yet reached its mature folded state.

In search of clues on potential ZnPP-mechanisms of protein sequestration, we sought the advice of various internationally recognized expert heme/porphyrin chemists and biochemists and porphyria experts on the possible mechanistic causes. Not a single investigator was aware that ZnPP caused protein aggregation, much less I κ B α -sequestration. ZnPP (along with SnPP), is actually believed to be safe and is recommended for the treatment of neonatal jaundice due to its effective inhibition of microsomal heme oxygenase (HO1), the key rate-limiting enzyme in the conversion of heme to biliverdin [9]. However, *in vivo*, overproduction of protoporphyrin IX (PPIX) due to defects in ferrochelatase (congenital erythropoietic protoporphyria) or PPIX-overproduction in X-linked protoporphyria, as well as iron-deficiency or lead-poisoning induced anemias (that can exhaust iron-stores) leads to ZnPP-generation [10-12]. Our findings suggest that under these conditions, these patients may easily succumb to ZnPP-elicited I κ B α -sequestration and consequently unabated hepatic NF- κ B-elicited activation of cytokines and chemokines. We believe, these findings would for the first-time alert physicians of this pathological potential of ZnPP and are clinically relevant not just in MDB-inducing diseases but also in clinical protoporphyrias and iron-deficiency/lead-induced anemias.

Supplementary methods

Contact for reagent and resource sharing

Information and requests for resources and reagents should be directed to M. A. Correia (almira.correia@ucsf.edu).

Experimental model details

Animal studies:

C57BL/6 wild type male mice (8-12-week old) purchased from the Jackson Laboratory (Bar Harbor, ME). Mice were fed a standard chow-diet and maintained under a normal diurnal light cycle. All animal experiments were carried out strictly by protocols specifically approved by the UCSF/Institutional Animal Care and Use Committee (IACUC) and its care and use of laboratory animal guidelines. For the ZnPP-treatment, ZnPP was dissolved in sterile DMSO at 100 mM, and then diluted 1:10 (v:v) with sterile 7.5% BSA to a final concentration of 10 mM. Mice were weighed and then injected daily with either ZnPP (50 $\mu\text{mol/kg}$, i.p.), or vehicle (controls) (10% DMSO in 7.5% BSA) for 7 days. Liver samples were collected and frozen at -80°C until RNA isolation.

Cell culture:

All cells were grown at 37°C with 5% CO_2 in a humidified incubator. C57BL/6 wild type male mice (8-12-week old) purchased from the Jackson Laboratory (Bar Harbor, ME) were used for primary hepatocyte preparation. Hepatocytes were isolated by *in situ* collagenase perfusion and purified by Percoll-gradient centrifugation by the UCSF Liver Center Cell Biology Core, as described previously [13]. Fresh primary mouse hepatocytes were cultured on Type I collagen-coated 60 mm Permax plates (Thermo Scientific, Grand Island, NY) in William's E Medium supplemented with 2 mM L-glutamine, insulin-transferrin-selenium, 0.1% bovine albumin Fraction V, Penicillin-Streptomycin and 0.1 μM dexamethasone. Cells were allowed to attach for 4 to 6 h and then overlaid with Matrigel. From the 2nd day after plating, the medium was replaced daily, and cells were further cultured for 4-5 days with daily light microscopic examination for any signs of cell death and/or cytotoxicity. On day 5, some cells were treated with 30 μM NMPP (dissolved in DMSO), 10 μM PPIX (dissolved in DMSO with sonication) or 10 μM zinc (II)-PPIX (ZnPP, dissolved in DMSO and complexed with bovine serum albumin (BSA) at a molar ratio of 4:1 to keep it solubilized in the medium) for various times as indicated (Results). In some cases, hepatocytes were pretreated with various inhibitors as indicated (Results) for 1 h before treatment with NMPP, PPIX or ZnPP.

HepG2 and HeLa cells were cultured in minimal Eagle's medium (MEM) containing 10% v/v fetal bovine serum (FBS) and supplemented with nonessential amino acids and 1 mM sodium pyruvate. HEK293T and MEF cells were cultured with Dulbecco's Modified Eagle high glucose medium (DMEM) containing 10% v/v FBS. For transfection experiments, cells were seeded onto 6-well plates, and when cells were 60% confluent, each cell well was transfected with 3 μg plasmid DNA complexed with TurboFect transfection reagent for HEK293T cells and X-tremeGENE HP transfection reagent for HepG2 cells according to the manufacturers'

instructions. At 40-72 h after transfection, cells were either treated as indicated or directly harvested for assays.

Method details

Hepatic PPIX content: PPIX content was determined using the intrinsic PPIX fluorescence as described [14]. Briefly, 50 μ l of cell lysates were first extracted with 400 μ l of EtOAc-HAc (3:1) and then re-extracted with another 400 μ l of EtOAc-HAc. The extracts were pooled and reextracted with 400 μ l of 3 M HCl. After centrifugation, the aqueous phase was recovered for fluorescent determination in a SpectrumMax M5 plate reader at an excitation 405 nm. The intensity at emission 610 nm was quantified relative to a standard curve prepared with known concentrations of pure PPIX.

Plasmids: The primers, templates, vectors and restriction enzymes (RE) used for constructing plasmids used in this study are summarized below:

Plasmid	Template	PCR primers (restriction sites underlined)	Vector	RE
C1-Emerald-lkB α	pCMV-3HA-lkB α	GCTCA <u>AAGCTTC</u> Gttccaggcggccgagcg Ggaggccagcgtctgacggtatga <u>CCCGGGAT</u> CC	C1-Emerald	<i>HindIII</i> <i>SmaI</i>
pcDNA6-p62-Myc	cDNA clone (IMAGE:4298142)	<u>AAGCTT</u> atggcgtcgtcaccg gcatccccgccgttgc <u>CTCGAG</u>	pcDNA6.1 Myc/His ₆	<i>HindIII</i> <i>XhoI</i>
pcDNA3-NBR1	cDNA clone (IMAGE:2989212)	TAGACTCGAGGCCACC <u>atgga</u> accacag <u>gttactc</u> ctggtacagccaacgctattga <u>CTCGAGTCTA</u>	pcDNA3.1	<i>XhoI</i> <i>KpnI</i>

Electrophoretic mobility shift assay (EMSA): Nuclear fractions of cells were prepared using NE-PER Nuclear and Cytoplasmic Extraction Reagents. EMSA were performed using LightShift Chemiluminescent EMSA Kit. Briefly, 2-5 μ g of nuclear extracts were incubated with 1 μ l of biotin-labeled NF κ B DNA probes in binding buffer [10 mM Tris, pH 7.5, 50 mM KCl, 1 mM DTT, 5 mM MgCl₂, 0.2 mM EDTA, 5% glycerol, 0.5% NP-40, 1 μ g of poly dl-dC]. The final volume of the mixture was adjusted to 20 μ l and incubated at room temperature for 30 min, and then mixed with 5 μ l of loading buffer for loading onto 5% TBE Polyacrylamide Gel (Biorad, Hercules, CA). The gel was run at 120 V until the dye reached the gel bottom, and then transferred to Hybond-N+ positively charged nylon membrane (GE Life Sciences, Marlborough, MA). The NF- κ B complex shifted probes were detected by blotting with HRP-coupled streptavidin. For super-shift EMSA, the binding mixture (in the absence of the biotin-labeled probes) was first incubated with p65 antibody for 20 min on ice, and then the biotin-labeled probes were added and further incubated at room temperature for another 30 min before gel loading.

RNA isolation and semi-quantitative RT-PCR: Total RNA was extracted using RNeasy Mini Kit according to the manufacturers' instructions. Total RNA (2 μ g) was used to perform reverse transcription using SuperScript VILO Master Mix in a 20 μ l-reaction. Reverse transcribed first strand cDNA (1 μ l) was used in PCRs.

Western Immunoblotting (IB) Analyses: For Western IB analysis, whole-cell extracts were prepared with Cell Lysis buffer containing 20 mM Tris-HCl (pH 7.5), 150 mM NaCl, 1 mM EDTA, 1 mM EGTA, 1% Triton, 2.5 mM sodium pyrophosphate, 1 mM β -glycerophosphate, 1 mM Na₃VO₄, 1 μ g/ml leupeptin and supplemented with 10% glycerol and protease/phosphatase inhibitor cocktail. Cell lysates were sonicated for 10s and then cleared by centrifugation at 4°C in a tabletop centrifuge at the highest speed for 10 min. Protein concentrations were determined by BCA assay and equal amounts of proteins were separated on 4-15% Tris-Glycine eXtended (TGX) polyacrylamide gels. Proteins were transferred onto nitrocellulose membranes (Biorad, Hercules, CA) for IB analyses. The antibodies used are listed in Key Resources Table.

Co-Immunoprecipitation (Co-IP) analyses: Whole-cell extracts were prepared as described above. Cell lysates (1 mg) were then incubated with indicated antibodies (2 μ g) or control IgGs at 4°C overnight. Antibody-antigen complexes were then captured by protein G Dynabeads at room temperature for 1 h, and then eluted by heating at 95°C for 10 min in 2X SDS-loading buffer. Eluates were subjected to IB analyses as described above.

Sequential solvent extraction of cell lysates: Cells were harvested in cell lysis buffer as described above and the cell lysates were cleared by centrifugation at 14,000g. The pellet was then solubilized in RIPA buffer supplemented with 0.1% SDS, 10% glycerol and protease/phosphatase inhibitor cocktail with sonication followed by centrifugation at the highest speed for 10 min. The resulting pellet was then solubilized with sonication in urea/CHAPS buffer containing 8 M urea, 2 M thiourea, 4% CHAPS, 20 mM Tris-base, and 30 mM DTT and supplemented with protease/phosphatase inhibitor cocktail. High salt buffer (HSB)-extraction (Fig. 4C) was carried out as described previously [15]. Briefly, cells were first harvested in cell lysis buffer containing 1% Triton as described above, the resulting pellet was then suspended in a cell lysis buffer supplemented with 1.5 M KCl (HSB) with sonication. Upon sedimentation, the resulting pellet was solubilized in Laemmli buffer containing 4% SDS or in urea/CHAPS buffer as described above.

Confocal Immunofluorescence microscopy (CIFM): Cells were grown on collagen-coated glass coverslips and treated as indicated. Cells were fixed with 4% formaldehyde for 20 min at room temperature followed by methanol at -20°C for 1 min. After that, cells were rinsed with PBS and blocked for 1 h with 10% normal goat serum in PBS /0.1% Tween at room temperature, and then stained with indicated primary antibodies at 4°C overnight. Cells were then washed in PBS 0.1% Tween three times and then stained with secondary antibodies for 1 h at room temperature. Cells were further washed three times in PBS 0.1% Tween and then mounted using ProLong Diamond Antifade Mountant with DAPI nuclear stain (Molecular Probes, Grand Island, NY). The following secondary antibodies were applied: Goat anti-rabbit IgG Alexa Fluor 488 (Invitrogen, Grand Island, NY), anti-mouse IgG Alexa Fluor 647 (Cell Signaling Technology, Danvers, MA). These particular fluor dyes were selected to circumvent any specific interference from ZnPP intrinsic fluorescence. Images were taken with a Nikon Yokogawa CSU-22 Spinning Disk Confocal Microscope using a Plan Apo VC 100x/1.4 oil lens or on a Nikon high-speed wide-field Andor Borealis CSU-W1 spinning disk confocal microscope using a Plan Apo VC 60x/1.4 oil lens. Images were processed using ImageJ software. For quantification, at least 600 cells at each condition were evaluated. Statistical significance was tested using two-sided unpaired Student's t-test.

Immunoaffinity purification (IAP): We employed high-affinity alpaca Nanobody crosslinked beads (GFP-Trap) for IAP, which not only enabled a high-level enrichment of target proteins but

also eliminated IgG contaminants that confound downstream LC-MS/MS analyses. N-terminally mEmerald (GFP)-tagged I κ B α (GFP-I κ B α) was transiently transfected into HEK293T cells, with mEmerald-transfected cells as background control (C1-GFP). Two wells of HEK293T cells grown on 6-well plates were pooled and lysed in 1 ml lysis buffer supplemented with 10% glycerol, protease/phosphatase inhibitor cocktail and 20 mM N-ethylmaleimide (NEM). Centrifugation-cleared cell lysates were incubated with 50 μ l GFP-trap agarose beads at 4°C overnight. Subsequently, GFP-trap beads were collected by centrifugation at 3,000g for 30s and then washed 5 times with cell lysis buffer. Co-immunoprecipitated proteins were eluted by incubating beads with 2X Laemmli buffer at 70°C for 15 min. Eluates were then subjected to SDS-PAGE and stained with Coomassie Blue to visualize the bands for subsequent in-gel digestion.

Biotinylation by antibody-recognition (BAR): Traditional approaches for in vivo protein-protein interactions such as co-IP are based on affinity capture of stable protein complexes that will be disrupted under harsh denaturing conditions. By contrast, biotinylation proximity labeling circumvents this limitation by introducing an enzyme to the target protein that can generate distance-constrained reactive biotin molecules to covalently link neighboring proteins, providing a permanent tag that survives purification under harsh conditions for downstream identification [16]. We chose BAR/APEX over BioID (the two popular methods for in vivo biotinylation proximity) because the BAR approach [17] is much more robust as it enables quicker capture of interacting proteins (as the peroxidase mediated biotinylation takes only a few minutes) without the more protracted BioID methodology (requiring 18-24 h tagging time), which could overlook short-term/transient interactants. BAR analyses were performed according to [17]. Briefly, two wells of HEK293T cells grown on collagen-coated 6-well plates were first treated as indicated and then fixed with 4% formaldehyde for 10 min at room temperature and permeabilized for 7 min with 0.5% Triton-X in PBS. After rinsing with PBS, cells were incubated with 0.5% H₂O₂ for 10 min. After rinsing with PBS, cells were then blocked for 1 h with 10% normal goat serum in PBS/0.1% Tween, and then stained with I κ B α antibody (mouse monoclonal, 44D4) at a 1:100 dilution in 1% normal goat serum in PBS/0.1% Tween at 4°C overnight. Negative control staining with no antibody was also performed. Cells were then washed in PBS 0.1% Tween for over 1 h with at least 5 buffer changes and then stained with secondary poly-HRP-conjugated goat anti-mouse IgGs (from Biotin XX Tyramide SuperBoost™ Kit) at a 1:1000 v:v dilution in 1% normal goat serum in PBS/0.1% Tween for 1 h. Cells were further washed for over 2 h in PBS 0.1% Tween with at least 5 buffer changes. After that, cells were labeled with biotin using Biotin XX Tyramide SuperBoost™ Kit following product instructions. Briefly, cells were pre-incubated with 300 ml of reaction buffer containing biotin-XX-tyramide (Biotin-Phenol) for 15 min; H₂O₂ was then added to obtain a final concentration of 0.5 mM and incubated for another 5 min. Negative controls without H₂O₂ were also included. The labeling reaction was then stopped by quickly exchanging the reaction solution with 1 ml of 500mM sodium ascorbate. Cells were washed 3 times with PBS and then lysed in RIPA buffer supplemented with 2% SDS and boiled for 1 h to reverse formaldehyde crosslinking. The cell lysates were cleared by centrifugation at 14,000g, the supernatants were used as whole cell lysates (WCL). The resulting pellet was further solubilized in urea/CHAPS buffer as described above. Aliquots from both fractions were used for streptavidin-HRP blot (Invitrogen, Grand Island, NY, #S911), to characterize the specificity and efficiency of BAR. The remaining WCL and urea/CHAPS fractions were separately diluted 1:2 (v:v) in RIPA buffer for streptavidin (SA) pull-down. SA pull-downs were performed according to [18]. Briefly, 50 μ l of streptavidin magnetic beads were added to the lysates to incubate at 4°C overnight on a rotator. Beads were then washed twice with RIPA buffer, once with 1 M KCl, once with 2 M urea in 20 mM Tris base, and lastly, twice with RIPA buffer. Biotinylated proteins were then eluted by incubating beads in 40 μ l of 2X Laemmli buffer

supplemented with 2 mM biotin at 95°C for 5 min. Eluates were then subjected to SDS-PAGE and stained with Coomassie Blue to visualize the bands for subsequent in-gel digestion. For SA pull-down from urea/CHAPS fractions, the last 2 washes were performed using 100 mM ammonium bicarbonate (ABC) before proceeding with on-beads digestion.

Mass spectrometry (MS): For in-gel digestion, each gel lane was sliced into 8-10 sections and processed separately using a standard in-gel digestion procedure [19, 20]. Briefly, each gel piece was reduced and alkylated, and then digested overnight with 300 ng of Trypsin/Lys-C Mix (Promega, Madison, WI). For on-bead digestion after SA pull-down, beads were first resuspended in 6 M urea in 100 mM ABC, and reduced by adding final 10 mM DTT and incubation at 37°C for 30 min. The samples were then alkylated by adding final 15 mM iodoacetamide with incubation at room temperature in the dark for 30 min. Trypsin/Lys-C Mix (100 ng) was then added and the mixture incubated for 4 h at 37°C. The mixture was then diluted 1:6 (v:v) with 100 mM ABC to reduce the urea concentration to 1 M and then further incubated at 37°C overnight. The resulting peptide mixture was desalted using C18-Zip tips (Millipore, Hayward, CA), speed-vacuumed to dryness and suspended in 0.1% formic acid for injection into an LTQ-Orbitrap Velos mass spectrometer (Thermo Fisher, Grand Island, NY) coupled to a nano-Acquity UPLC (Waters, Milford, MA) with an EASY-Spray column (75 μ m x 15 cm column packed with 3 μ m, 100 Å PepMap C18 resin; Thermo Scientific, Grand Island, NY). Each sample was separated on the column following a 90-min solvent gradient (Solvent A: Water/0.1% formic acid; Solvent B: Acetonitrile/0.1% formic acid) and the mass spectrometer was operated under high-energy collisional dissociation (HCD) mode. Peak lists were extracted using PAVA, an in-house software developed by UCSF Mass Spectrometry facility. Peak lists from 8-10 mass spectrometric fractions under each experimental condition were pooled to search against the Swissprot human database (SwissProt.2015.12.1; 20194/549832 entries searched) using ProteinProspector (version 5.19.1; <http://prospector.ucsf.edu/prospector/mshome.htm>) [21]. A fully randomized database was used to estimate false discovery rates (FDR) [22]. Score thresholds were chosen at <1% FDR at the peptide level. ProteinProspector search parameters were as follows: Tolerance for precursor and product ions were 20 ppm and 25 ppm; a maximum of 1 missed cleavage of trypsin was allowed; carbamidomethylation of cysteine was set as a fixed modification; variable modifications include: N-terminal Met loss and/or acetylation, Met oxidation, peptide N-terminal Gln to pyroGly conversion; number of variable modifications was 2. Reporting thresholds were as follows: Minimum score of protein: 22.0; minimum score of peptide: 15.0; maximum E value of protein: 0.01; maximum E value of peptide: 0.05.

Mass spectral data processing: To obtain a high-confidence I κ B α -interactome, three independent IAP-MS experiments were performed, (from cell transfection, IAP to MS protein identification), each consisting of three biological replicates (three wells each individually transfected). The identified proteins were strictly filtered as follows: 1) From each LC-MS/MS run, only proteins with two or more peptides identified were utilized for further analyses; 2) when some unique peptides matched to multiple protein isoforms, only the isoform with the highest number of matched peptides was reported; 3) only proteins that were immunoaffinity purified with mEmerald-I κ B α in all three replicates were kept for further analyses. After filtering, an enrichment ratio of total spectral counts for each protein in mEmerald-I κ B α IAP over GFP (C1-mEmerald) background control was calculated as described [23]. Proteins that were not detected in the background control were artificially assigned 0.5 spectral counts, so that an enrichment fold could be calculated. Only proteins that were enriched \geq 2-fold in all three

replicates were considered high-confidence interactors. Mean ratio and p-value from three replicates were then obtained. p-values were obtained using a paired Student's t-test with total spectral counts from GFP-control compared to mEmerald-I κ B α IAP values. To characterize the aggregate-proteome, proteins in high molecular mass (HMM)-regions and urea/CHAPS-solubilized fractions from HEK293T and HepG2 cells were similarly filtered and those in ZnPP-treated and control samples were directly compared. Identified proteins were filtered as described above. Overlap analyses were performed using the Venn Diagram tool (<http://bioinformatics.psb.ugent.be/webtools/Venn/>).

Network analysis of aggregated proteins: 192 commonly found proteins in ZnPP-induced aggregates from both cell lines were searched against a STRING database version 10.0 [24] for protein-protein interactions. We used the highest confidence score (≥ 0.9) to obtain a protein-interaction network. The network was exported to Cytoscape software [25] for pathway annotation and visualization.

siRNA-knockdown analyses: HEK293T cells were transfected using DharmaFECT 4 Transfection Reagent, with 10 nM siRNA specific for RanBP2 or NUP153. Treatments were performed 48 h after transfection. HepG2 cells were transfected using DharmaFECT 4 Transfection Reagent with 50 nM siGENOME Human NFKBIA siRNA-Smartpool or control non-targeting siRNA. Primary mouse hepatocytes, were transfected using DharmaFECT 4 Transfection Reagent with 50-100 nM siGENOME Nfkbia siRNA-SMARTpool or control siRNA non-targeting siRNA, 16 h before overlay with Matrigel. Cells were harvested 72-96 h after transfection.

Bioinformatic Analyses

GRAVY scores estimating average hydrophobicity was calculated using Kyte and Doolittle hydrophobicity analyses (<http://web.expasy.org/protparam/>) [26]. Positive GRAVY scores suggest more hydrophobicity. Proteins with long intrinsically disordered regions was predicted using SLIDER method (<http://biomine.cs.vcu.edu/servers/SLIDER/>) [27]. This computational method is based on the physicochemical properties of amino acids, sequence complexity, and amino acid composition, a SLIDER score >0.538 suggests a high likelihood that the protein contains a long (>30 residues) disordered segment.

Quantification and statistical analyses

Statistical significance was tested using the two-sided unpaired Student's t-test. N, number of individual experiments, was indicated in each figure legend.

Table 1. Structural properties of the 47 I κ B α -interacting and ZnPP-inducible-aggregating proteins.

Gene	Accession	GRAVY	SLIDER	Protein Name
NUP153	P49790	-0.469	0.869	Nuclear pore complex protein Nup153
NUP155	O75694	-0.129	0.701	Nuclear pore complex protein Nup155
IMMT	Q16891	-0.465	0.835	MICOS complex subunit MIC60
EPRS	P07814	-0.517	0.825	Bifunctional glutamate/proline--tRNA ligase
EIF3A	Q14152	-1.489	0.946	Eukaryotic translation initiation factor 3 subunit A
LRPPRC	P42704	-0.206	0.723	Leucine-rich PPR motif-containing protein, mitochondrial
LBR	Q14739	-0.056	0.651	Lamin-B receptor
DDOST	P39656	-0.057	0.417	Dolichyl-diphosphooligosaccharide--protein glycosyltransferase 48 kDa subunit
RANBP2	P49792	-0.596	0.840	E3 SUMO-protein ligase RanBP2
ABCD3	P28288	-0.13	0.518	ATP-binding cassette sub-family D member 3
PDCD6IP	Q8WUM4	-0.468	0.785	Programmed cell death 6-interacting protein
MDN1	Q9NU22	-0.371	0.898	Midasin
RPS2	P15880	-0.233	0.562	40S ribosomal protein S2
MSH6	P52701	-0.499	0.836	DNA mismatch repair protein Msh6
KIF5B	P33176	-0.81	0.876	Kinesin-1 heavy chain
COPB1	P53618	-0.091	0.684	Coatomer subunit beta
USP7	Q93009	-0.643	0.722	Ubiquitin carboxyl-terminal hydrolase 7
RPL10	P27635	-0.553	0.458	60S ribosomal protein L10
HADHA	P40939	-0.078	0.595	Trifunctional enzyme subunit alpha, mitochondrial
DDX6	P26196	-0.323	0.674	Probable ATP-dependent RNA helicase DDX6
TRIM28	Q13263	-0.387	0.857	Transcription intermediary factor 1-beta
COPG1	Q9Y678	-0.145	0.658	Coatomer subunit gamma-1
RPL8	P62917	-0.528	0.539	60S ribosomal protein L8
HACD3	Q9P035	0.003	0.390	Very-long-chain (3R)-3-hydroxyacyl-CoA dehydratase 3
NUP93	Q8N1F7	-0.366	0.705	Nuclear pore complex protein Nup93
HADHB	P55084	-0.072	0.528	Trifunctional enzyme subunit beta, mitochondrial
MCM3	P25205	-0.564	0.879	DNA replication licensing factor MCM3
POLR1C	O15160	-0.28	0.416	DNA-directed RNA polymerases I and III subunit RPAC1
CAND1	Q86VP6	-0.019	0.750	Cullin-associated NEDD8-dissociated protein 1
EIF3M	Q7L2H7	-0.184	0.544	Eukaryotic translation initiation factor 3 subunit M
SLC25A11	Q02978	0.117	0.301	Mitochondrial 2-oxoglutarate/malate carrier protein
BIRC6	Q9NR09	-0.138	0.870	Baculoviral IAP repeat-containing protein 6
PSMA4	P25789	-0.459	0.609	Proteasome subunit alpha type-4
GTF2I	P78347	-0.526	0.798	General transcription factor II-I
IK	Q13123	-1.427	0.928	Protein Red
SLC25A10	Q9UBX3	0.148	0.327	Mitochondrial dicarboxylate carrier
KPNB1	Q14974	-0.092	0.704	Importin subunit beta-1
RPS6	P62753	-0.945	0.820	40S ribosomal protein S6
RPL7A	P62424	-0.547	0.685	60S ribosomal protein L7a
PSMD3	O43242	-0.529	0.821	26S proteasome non-ATPase regulatory subunit 3
SEC16A	O15027	-0.607	0.924	Protein transport protein Sec16A
SEC23A	Q15436	-0.238	0.552	Protein transport protein Sec23A
RPS8	P62241	-1.02	0.651	40S ribosomal protein S8
MCM5	P33992	-0.352	0.671	DNA replication licensing factor MCM5
GTF3C3	Q9Y5Q9	-0.363	0.858	General transcription factor 3C polypeptide 3
IPO4	Q8TEX9	0.07	0.797	Importin-4
XRN2	Q9H0D6	-0.651	0.790	5'-3' exoribonuclease 2
NFKBIA	P25963	-0.452	0.8195	NF-kappa-B inhibitor alpha
NFKBIB	Q15653	-0.388	0.7360	NF-kappa-B inhibitor beta
NFKBIE	O00221	-0.4336	0.8077	NF-kappa-B inhibitor epsilon
SQSTM1	Q13501	-0.632	0.6246	Sequestosome-1

* The GRAVY number of a protein is a measure of its hydrophobicity or hydrophilicity. The hydrophathy values range from -2 to +2 for most proteins, with the positively rated proteins being more hydrophobic. Less hydrophobic proteins are labeled red. ** Proteins are listed with SLIDER score, the higher the score the more likely a protein has a long (≥ 30 AAs) disordered segment. Scores above 0.538 indicates that a given protein has a long disorder segment (labeled red).

References:

- [1] Jiang HY, Wek SA, McGrath BC, Scheuner D, Kaufman RJ, Cavener DR, et al. Phosphorylation of the alpha subunit of eukaryotic initiation factor 2 is required for activation of NF-kappaB in response to diverse cellular stresses. *Mol Cell Biol* 2003;23:5651-5663.
- [2] Deng J, Lu PD, Zhang Y, Scheuner D, Kaufman RJ, Sonenberg N, et al. Translational repression mediates activation of nuclear factor kappa B by phosphorylated translation initiation factor 2. *Mol Cell Biol* 2004;24:10161-10168.
- [3] Chen JJ. Regulation of protein synthesis by the heme-regulated eIF2alpha kinase: relevance to anemias. *Blood* 2007;109:2693-2699.
- [4] Cuervo AM, Hu W, Lim B, Dice JF. I kappa B is a substrate for a selective pathway of lysosomal proteolysis. *Mol Biol Cell* 1998;9:1995-2010.
- [5] Pankiv S, Clausen TH, Lamark T, Brech A, Bruun JA, Outzen H, et al. p62/SQSTM1 binds directly to Atg8/LC3 to facilitate degradation of ubiquitinated protein aggregates by autophagy. *J Biol Chem* 2007;282:24131-24145.
- [6] Chen F, Lu Y, Kuhn DC, Maki M, Shi X, Sun SC, et al. Calpain contributes to silica-induced I kappa B-alpha degradation and nuclear factor-kappa B activation. *Arch Biochem Biophys* 1997;342:383-388.
- [7] Han Y, Weinman S, Boldogh I, Walker RK, Brasier AR. Tumor necrosis factor-alpha-inducible I kappa B-alpha proteolysis mediated by cytosolic m-calpain. A mechanism parallel to the ubiquitin-proteasome pathway for nuclear factor-kappa B activation. *J Biol Chem* 1999;274:787-794.
- [8] Cox TM. Protoporphyrin. In: Karl M. Kadish KMS, Roger Guilard, editor. *The Porphyrin Handbook: Medical aspects of porphyrins*. USA: Elsevier science; 2003.
- [9] Drummond GS, Kappas A. Prevention of neonatal hyperbilirubinemia by tin protoporphyrin IX, a potent competitive inhibitor of heme oxidation. *Proc Natl Acad Sci U S A* 1981;78:6466-6470.
- [10] Lamola AA, Yamane T. Zinc protoporphyrin in the erythrocytes of patients with lead intoxication and iron deficiency anemia. *Science* 1974;186:936-938.
- [11] Freeseemann AG, Gross U, Bensidhoum M, de Verneuil H, Doss MO. Immunological, enzymatic and biochemical studies of uroporphyrinogen III-synthase deficiency in 20 patients with congenital erythropoietic porphyria. *Eur J Biochem* 1998;257:149-153.
- [12] To-Figueras J, Millet O, Herrero C. Congenital Erythropoietic Porphyria. *Handbook of Porphyrin Science (Volume 29)*; 2013. p. 151-217.
- [13] Han XM, Lee G, Hefner C, Maher JJ, Correia MA. Heme-reversible impairment of CYP2B1/2 induction in heme-depleted rat hepatocytes in primary culture: translational control by a hepatic alpha-subunit of the eukaryotic initiation factor kinase? *J Pharmacol Exp Ther* 2005;314:128-138.
- [14] Chisolm J, Jr., Brown DH. Micro-scale photofluorometric determination of "free erythrocyte porphyrin" (protoporphyrin IX). *Clin Chem* 1975;21:1669-1682.
- [15] Ku NO, Toivola DM, Zhou Q, Tao GZ, Zhong B, Omary MB. Studying simple epithelial keratins in cells and tissues. *Methods Cell Biol* 2004;78:489-517.
- [16] Che Y, Khavari PA. Research Techniques Made Simple: Emerging Methods to Elucidate Protein Interactions through Spatial Proximity. *The Journal of investigative dermatology* 2017;137:e197-e203.
- [17] Bar DZ, Atkash K, Tavarez U, Erdos MR, Gruenbaum Y, Collins FS. Biotinylation by antibody recognition-a method for proximity labeling. *Nat Methods* 2018;15:127-133.
- [18] Hung V, Udeshi ND, Lam SS, Loh KH, Cox KJ, Pedram K, et al. Spatially resolved proteomic mapping in living cells with the engineered peroxidase APEX2. *Nat Protoc* 2016;11:456-475.

- [19] Rosenfeld J, Capdevielle J, Guillemot JC, Ferrara P. In-gel digestion of proteins for internal sequence analysis after one- or two-dimensional gel electrophoresis. *Anal Biochem* 1992;203:173-179.
- [20] Hellman U, Wernstedt C, Gonez J, Heldin CH. Improvement of an "In-Gel" digestion procedure for the micropreparation of internal protein fragments for amino acid sequencing. *Anal Biochem* 1995;224:451-455.
- [21] Chalkley RJ, Baker PR, Medzihradzky KF, Lynn AJ, Burlingame AL. In-depth analysis of tandem mass spectrometry data from disparate instrument types. *Mol Cell Proteomics* 2008;7:2386-2398.
- [22] Elias JE, Gygi SP. Target-decoy search strategy for increased confidence in large-scale protein identifications by mass spectrometry. *Nat Methods* 2007;4:207-214.
- [23] Ma H, McLean JR, Chao LF, Mana-Capelli S, Paramasivam M, Hagstrom KA, et al. A highly efficient multifunctional tandem affinity purification approach applicable to diverse organisms. *Mol Cell Proteomics* 2012;11:501-511.
- [24] Szklarczyk D, Franceschini A, Wyder S, Forslund K, Heller D, Huerta-Cepas J, et al. STRING v10: protein-protein interaction networks, integrated over the tree of life. *Nucleic Acids Res* 2015;43:D447-452.
- [25] Shannon P, Markiel A, Ozier O, Baliga NS, Wang JT, Ramage D, et al. Cytoscape: a software environment for integrated models of biomolecular interaction networks. *Genome Res* 2003;13:2498-2504.
- [26] Kyte J, Doolittle RF. A simple method for displaying the hydropathic character of a protein. *J Mol Biol* 1982;157:105-132.
- [27] Peng Z, Mizianty MJ, Kurgan L. Genome-scale prediction of proteins with long intrinsically disordered regions. *Proteins* 2014;82:145-158.

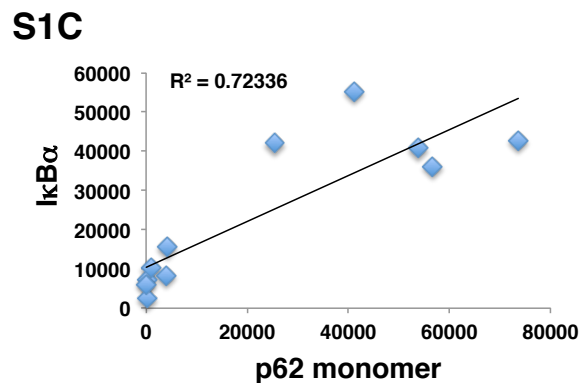
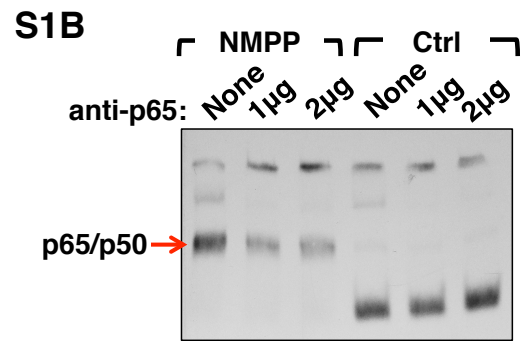
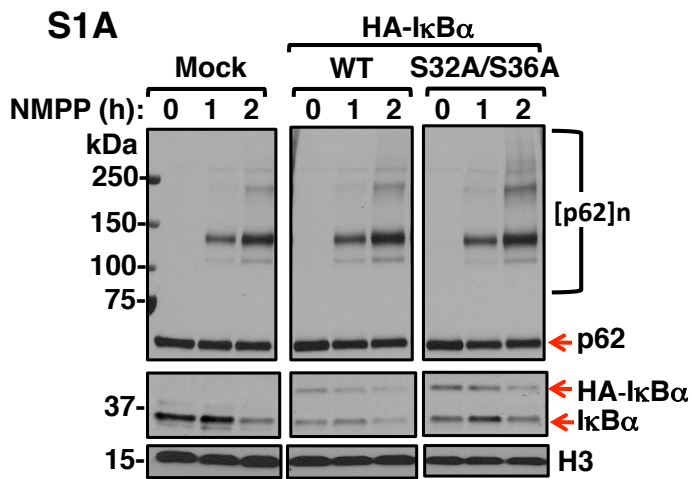
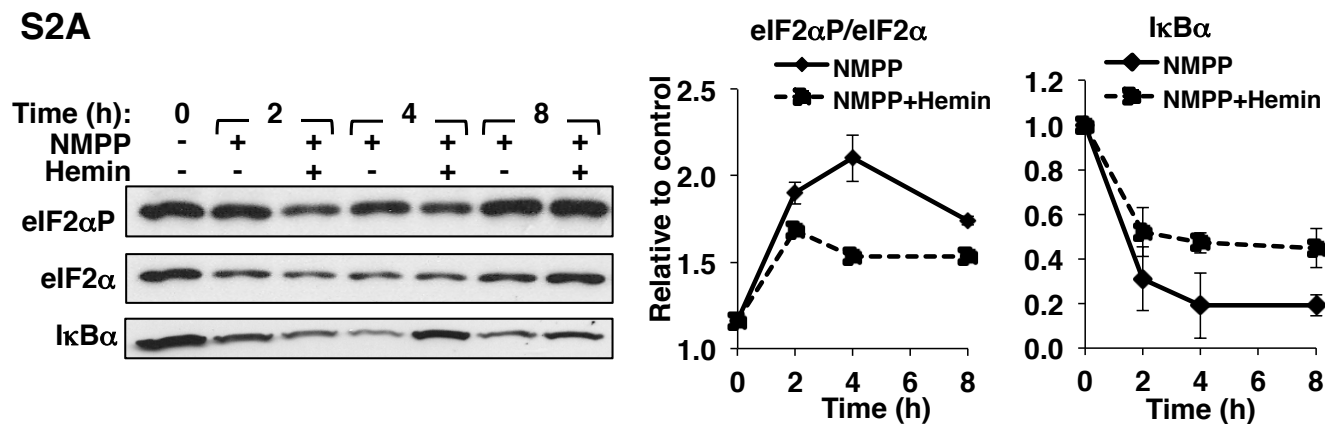
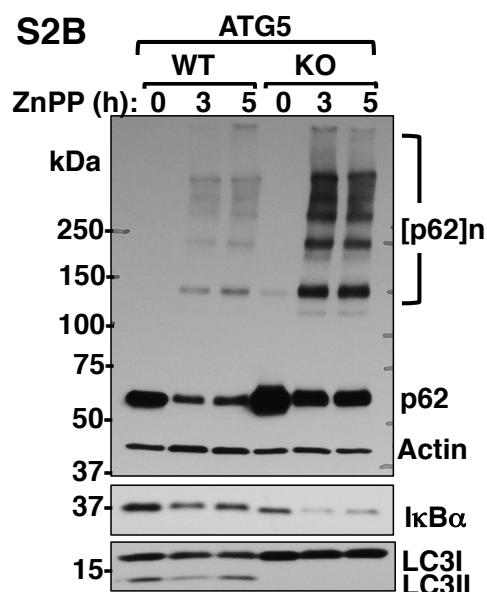


FIGURE S1. NMPP-elicited PPIX-accumulation with concurrent $\text{NF}\kappa\text{B}$ activation and $\text{I}\kappa\text{B}\alpha$ -loss is independent of proteasomal degradation, PPIX and ZnPP are even more potent elicitors of $\text{I}\kappa\text{B}\alpha$ -loss and p62-aggregation than NMPP (Related to Fig 1). A. HepG2 cells were transfected with pCMV4-3HA-IκBα or mutant pCMV4-3HA-IκBα-S32A/S36A for 40 h, then treated with NMPP for the indicated times. Cell lysates were subjected to IB analyses of p62 and IκBα with histone H3 as the loading control. **B.** Supershift EMSA using nuclear extracts from Fig 1D with p65-antibody verifies the identity of the p65/p50 band. **C.** The correlation of IκBα and p62 monomer levels quantified from Fig1E (n = 2).

S2A



S2B



S2C

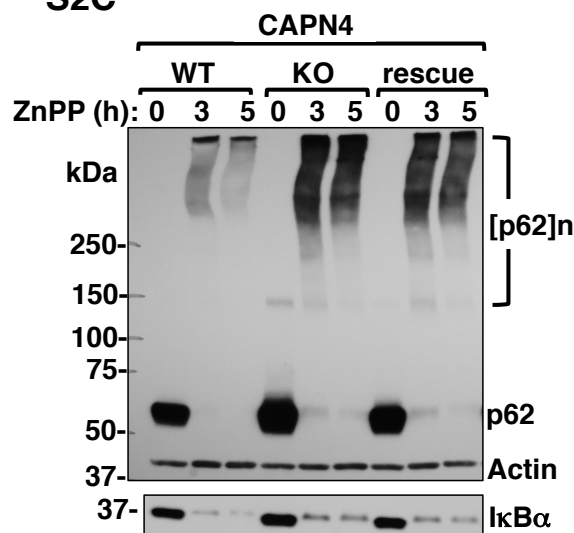


FIGURE S2. ZnPP-elicited IκBα loss is independent of heme deficiency elicited HRI-activation, autophagy and calpain-mediated proteolysis (Related to Fig 1). **A.** IB analyses of eIF2α, eIF2αP and IκBα in lysates from mouse hepatocytes treated with NMPP or NMPP plus hemin for the indicated times. The temporal profiles of the ratio of eIF2αP to total eIF2α as well as IκBα content were determined (Mean ± SD, n=3). **B.** ATG5 wild-type (ATG5WT) and knockout (ATG5KO) MEF cells were treated with 10 μM ZnPP for the indicated time. Cell lysates were used for IB analysis of p62, IκBα, and LC3, with actin as the loading control. **C.** MEF cells wild-type calpain (capn4WT), capn4 knockout (capn4KO) and capn4KO-rescue (wherein capn4 knockout cells were rescued by transfection of a Capn4 lentiviral vector) were treated with ZnPP for the indicated time. Cell lysates were used for IB analysis of p62 and IκBα with actin as the loading control.

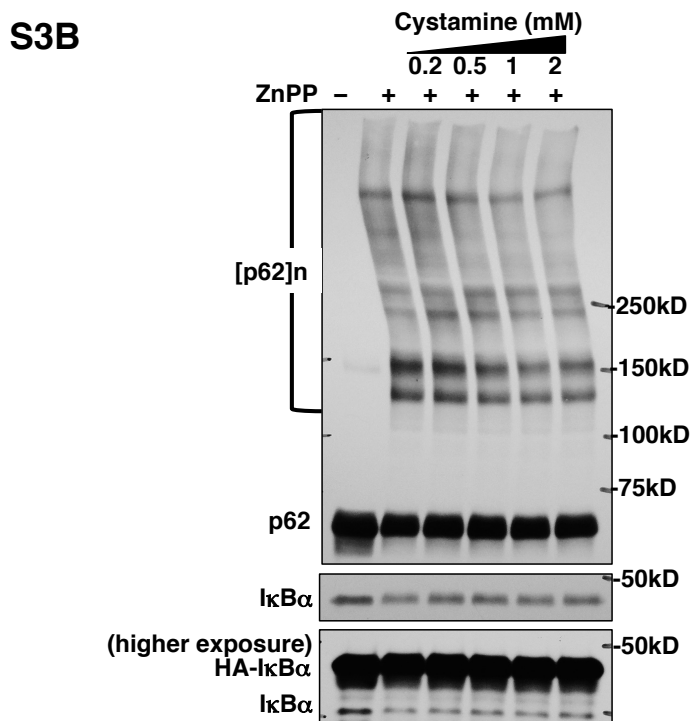
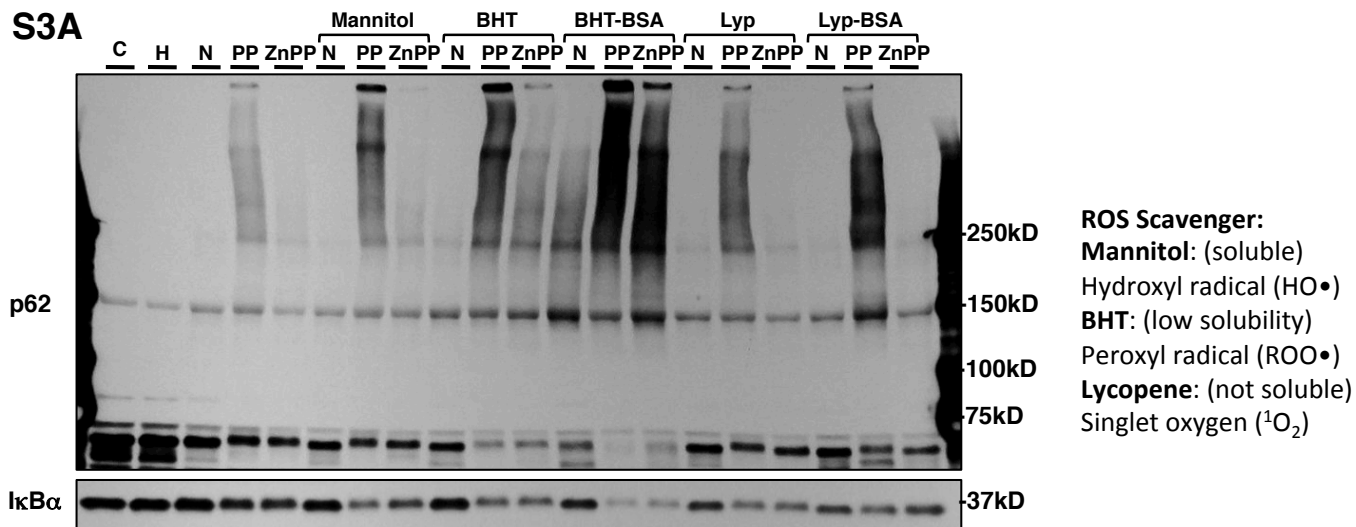


FIGURE S3. ZnPP-elicited IκBα loss and p62 cannot be reversed by antioxidants or TG2 inhibitors (Related to Fig 1). **A.** Primary mouse hepatocytes were left untreated, or pretreated for 1 h with 50mM mannitol, or 100μM BHT, or 50μM lycopene (Lyp), or BHT coupled with BSA to help keep it solubilized (BHT-BSA), or lycopene coupled with BSA (Lyp-BSA), and then treated with vehicle control (C), 10 μM hemin (H), 30 μM NMPP (N), or 10 μM PPIX (PP), or 10 μM ZnPP (ZnPP) for 4 h as indicated. Cell lysates were used for IB analyses of p62 and IκBα. **B.** HEK293T cells were co-transfected with pcDNA6-p62-myc or pCMV4-3HA-IκBα. 48 h after transfection, cells were pretreated with various concentrations of cystamine as indicated and then treated with 10 μM ZnPP for 2 h. Cell lysates were used for IB analyses of p62 and IκBα.

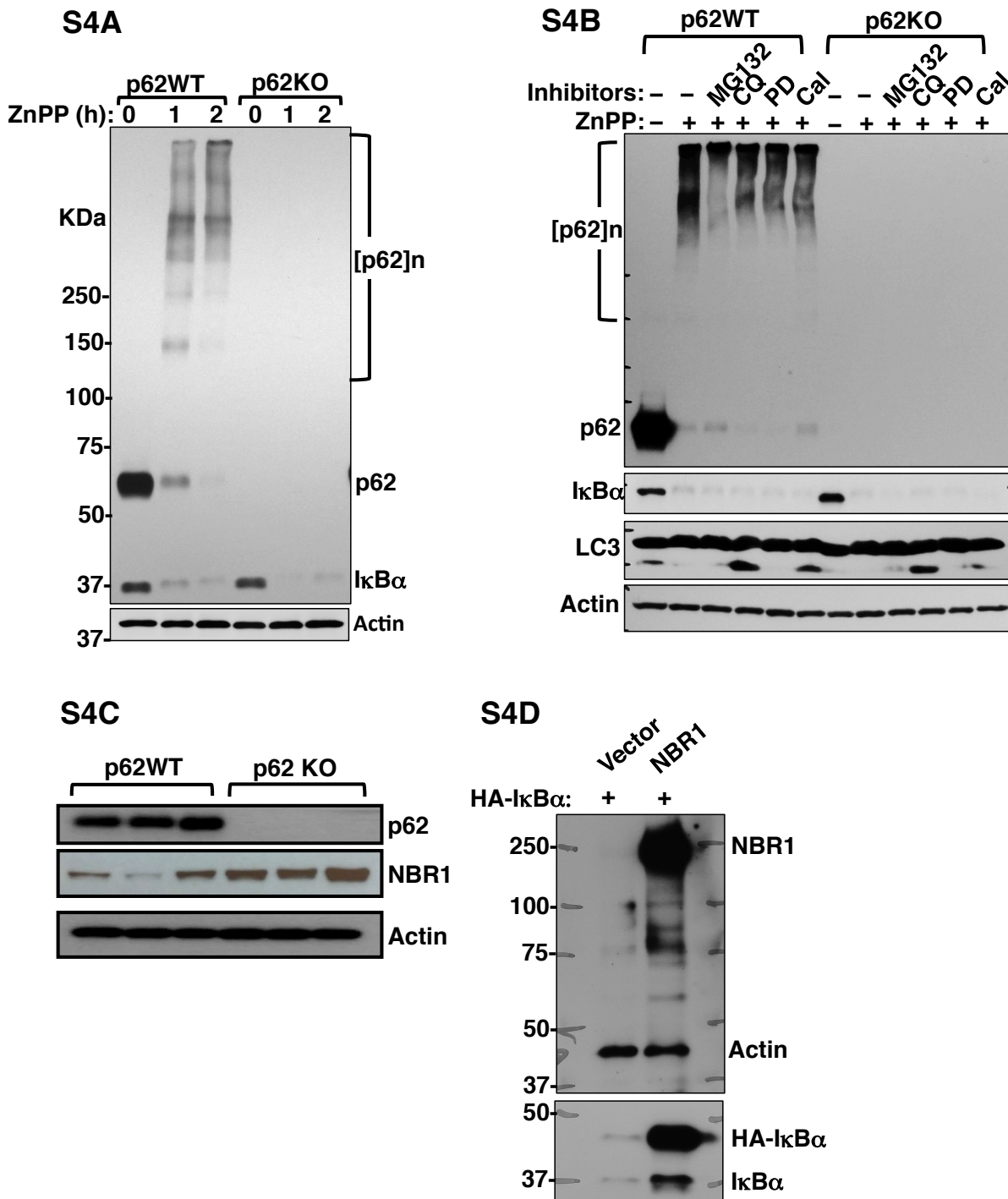


FIGURE S4. ZnPP-elicited $I\kappa B\alpha$ -loss is independent of NBR1 and other autophagic adaptors. (Related to Fig 2). A. p62WT and p62KO MEF cells were treated with 10 μ M ZnPP for the indicated times. Cell lysates were used for IB analyses of p62 and $I\kappa B\alpha$, with actin as the loading control. **B.** p62WT and p62KO MEF cells were pretreated for 1 h with inhibitors of various protein degradation pathways: MG132 (20 μ M; proteasomal), chloroquine (CQ, 100 μ M; lysosomal), PD150606 (PD, 200 μ M; calpain1/2), or calpeptin (Cal, 200 μ M; cathepsin and calpain), and then treated with 10 μ M ZnPP for 2 h. Cell lysates were used for IB analyses. **C.** Lysates from p62WT and p62KO primary mouse hepatocytes were used for IB analyses of p62, and NBR1 with actin as the loading control. The three lanes correspond to p62 WT and p62 KO hepatocytes from three individual mice. **D.** HEK293T cells were co-transfected with pCMV4-3HA- $I\kappa B\alpha$ with either pcDNA3 empty vector or pcDNA3-NBR1 for 48 h. Cell lysates were used for IB analyses of NBR1 and $I\kappa B\alpha$ with actin as the loading control.

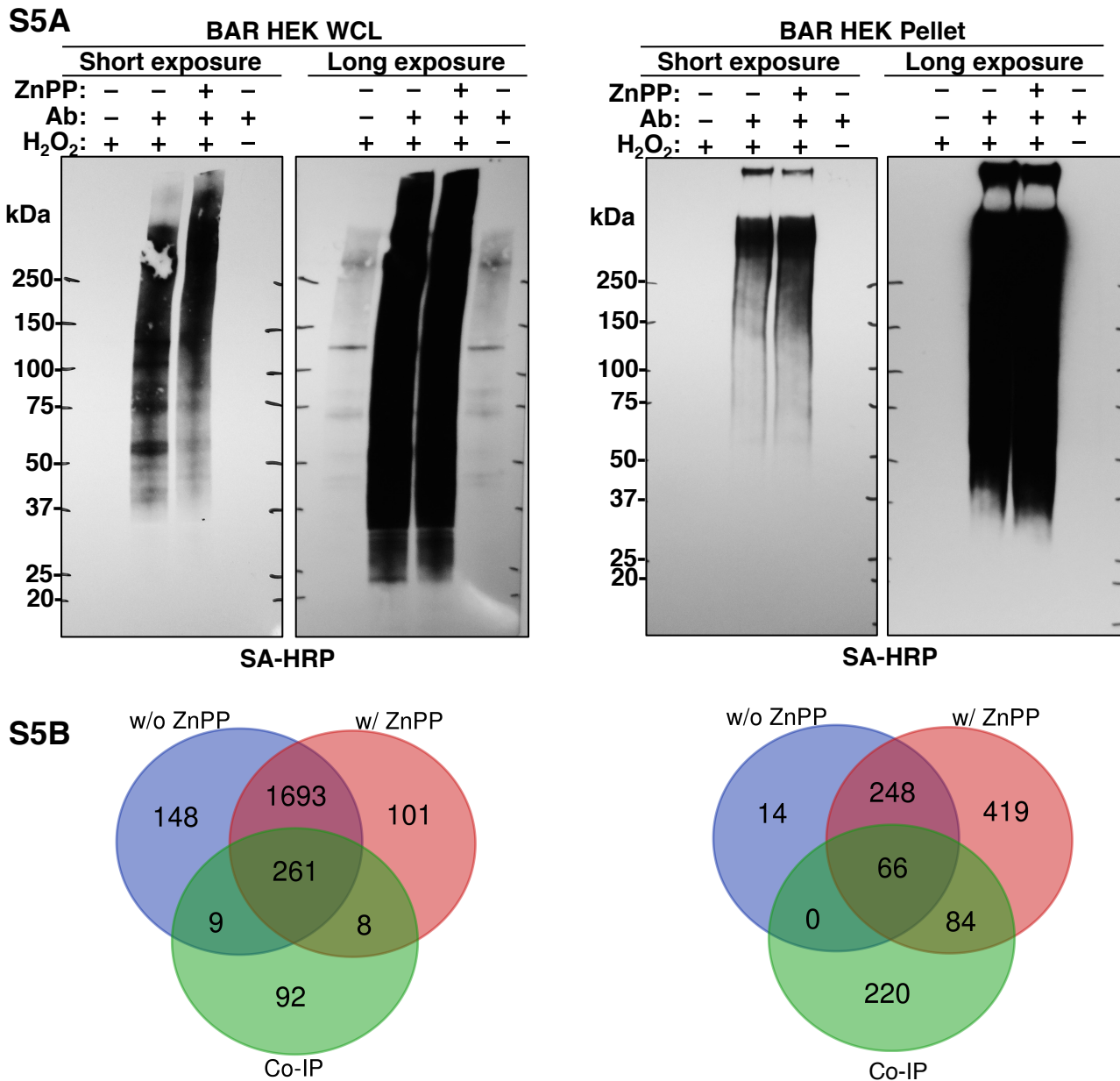


FIGURE S5. Characterization of biotinylation via $I\kappa B\alpha$ antibody recognition (BAR). (Related to Fig 5B). (A) HEK293T cells were transfected with with pCMV4-3HA- $I\kappa B\alpha$ for 48 h. Some cells were treated with 10 μ M ZnPP for 2 h. Cells were fixed and then stained with $I\kappa B\alpha$ antibody for downstream HRP antibody recognition dependent biotinylation labeling as described in Methods. Cells were lysed, sub-fractionated into whole cell lysates (WCL) and pellet as described in Methods, separated by SDS-PAGE and analyzed by blotting with streptavidin-HRP. Negative controls in which $I\kappa B\alpha$ antibody in substrate recognition or H₂O₂ in labeling reaction was omitted are shown in lanes 1 and 4 of each blot. The band pattern shows that biotinylation is dependent on the presence of both $I\kappa B\alpha$ antibody and H₂O₂, suggesting the specificity of biotinylation of endogenous $I\kappa B\alpha$ -proximal proteins. The up-shift of bands in WCL fraction and an increased intensity of bands in the pellet fraction in ZnPP treated cells suggest that $I\kappa B\alpha$ interacts with ZnPP-aggregated proteins. After higher exposure, in the negative control lanes from WCL fraction, some faint bands representing endogenous biotinylated proteins are detected (i.e. 130, 75 and 72 kDa). (B). Biotinylated proteins within each lysate (including negative controls) were then enriched using streptavidin-coated magnetic beads and trypsin/Lys-C digested for LC-MS/MS proteomic analyses. Non-specific protein binders were filtered out by comparison to negative controls, and only proteins with an enrichment ratio of ≥ 4 considered specifically biotinylated by BAR. The numbers of proteins identified using BAR in cells treated with or without ZnPP in comparison with the co-IP method in both fractions are shown in the Venn diagrams.